RSC Advances

PAPER

View Article Online
View Journal | View Issue

Cite this: *RSC Adv.*, 2026, **16**, 11458

Pyrazole/pyrimidine derivatives endowed with azobenzenes as dual EGFR^{T790M} and VEGFR-2 inhibitors: anticancer, docking, synthesis, design and ADMET assessments

Kurls E. Anwer, [a] Mohamed A. Abdelgawad,*[b] Felemban Athary Abdulhaleem M.,[c] Nour E. A. Abd El-Sattar, [ad] Ahmed El-morsy,[ef] Tamer Nasr, [gh] Mohammed Elmowafy,[i] Khaled El-Adl *[jk] and Naglaa M. Ahmed [l]

New pyrazole/pyrimidine derivatives endowed with azobenzenes were synthesized using microwave and traditional methods. Our compounds were assessed for cytotoxicity against HepG2, MCF-7, HCT-116 and A549 cell lines as dual inhibitors of EGFR^{T790M} and VEGFR-2. A docking study was carried out to show the binding affinities and orientations of our derivatives in the active sites of VEGFR-2 and EGFR^{T790M}. The data of the docking study were highly correlated with the biological data. The HCT116 and A549 cell lines were extremely affected by our derivatives. Derivative **12** showed the greatest activity against A549, HepG2, MCF-7 and HCT116 cells, with IC_{50} = 5.12, 6.77, 5.85 and 5.25 μM, respectively. It showed higher cytotoxicity than erlotinib (IC_{50} = 5.49, 7.73, 8.20 and 13.91 μM, respectively) and lower cytotoxicity than sorafenib (IC_{50} = 4.04, 4.00, 5.58 and 5.05 μM, respectively) against the tested cell lines. The cytotoxicity of the highly active derivatives **5**, **6**, **8**, **9**, **10** and **12** against the MCF-10 healthy cell lines was evaluated. The assessed derivatives showed low cytotoxicity against MCF-10 cells, with IC_{50} = 50.90–55.50 μM. Additionally, all derivatives were assessed as dual VEGFR-2 and EGFR^{T790M} inhibitors. Compounds **12**, **8** and **10** displayed very good inhibitions toward VEGFR-2, with IC_{50} = 0.90, 0.95 and 1.00 μM, respectively. Similarly, structures **12**, **8**, **10**, **5** and **9** showed strong EGFR^{T790M} inhibitions, with IC_{50} = 0.25, 0.30, 0.33, 0.35 and 0.40 μM, respectively. In addition, *in silico* ADMET predictions were calculated for the highly active derivatives **8**, **10** and **12** and correlated to Lipinski's rule of five using erlotinib and sorafenib as standard ligands. The results presented our derivatives as promising candidates for advanced manipulations to get more potent anticancer agents with advanced VEGFR-2 and EGFR^{T790M} inhibitions.

Received 20th November 2025
Accepted 12th February 2026

DOI: 10.1039/d5ra08997b

rsc.li/rsc-advances

1. Introduction

Cancer, one of the most serious diseases to threaten human life, is characterized as a rebound system of uncontrolled cellular growth.[1] Angiogenesis is essential for the survival and spread of tumor cells, which is a primary cause of cancer-related deaths. As a result, the importance of angiogenesis inhibition in cancer treatment is growing.[2] Signal transduction leads to endothelial cell proliferation, migration, survival, and new vessel formation involved in angiogenesis.[3] Through signal transduction,

[a]*Department of Chemistry, Faculty of Science, Ain Shams University, Abbassia, Cairo, Egypt*
[b]*Department of Pharmaceutical Chemistry, College of Pharmacy, Jouf University, Sakaka, 72388, Saudi Arabia. E-mail: mhmdgwd@ju.edu.sa*
[c]*Department of Biology, College of Sciences, Umm Al-Qura University, Makkah 21955, Saudi Arabia*
[d]*Basic & Medical Sciences Department, Faculty of Dentistry, Alryada University for Science & Technology, Egypt*
[e]*Pharmaceutical Organic Chemistry Department, Faculty of Pharmacy (Boys), Al-Azhar University, Nasr City, Cairo, 11884, Egypt*
[f]*Pharmaceutical Chemistry Department, College of Pharmacy, The Islamic University, Najaf, Iraq*
[g]*Department of Pharmaceutical Chemistry, Faculty of Pharmacy, Capital University (Formerly Helwan University), Ain-Helwan, Cairo 11795, Egypt*
[h]*Medicinal Chemistry Department, Faculty of Pharmacy, Egypt-Japan University of Science and Technology (E-JUST), Alexandria, 21934, Egypt*
[i]*Department of Pharmaceutics, College of Pharmacy, Jouf University, Sakaka 72388, Saudi Arabia*
[j]*Pharmaceutical Chemistry Department, Faculty of Pharmacy, Heliopolis University for Sustainable Development, Cairo, Egypt. E-mail: khaled.eladl@hu.edu.eg; eladlkhaled74@yahoo.com*
[k]*Pharmaceutical Medicinal Chemistry and Drug Design Department, Faculty of Pharmacy (Boys), Al-Azhar University, Nasr City, Cairo, 11884, Egypt. E-mail: eladlkhaled74@azhar.edu.eg*
[l]*Pharmaceutical Organic Chemistry Department, Faculty of Pharmacy, Capital University (Formerly Helwan University), Ain-Helwan, Cairo 11795, Egypt*

receptor tyrosine kinases control intra- and intercellular signaling. The regulation of vital cellular functions, such as growth, differentiation, survival, metabolism, and proliferation, is greatly influenced by these proteins.[4]

EGFR and VEGFR-2, as tyrosine kinases, are associated with several diseases and diverse cancer growth groups. They are closely related and share common signaling pathways, which are segmented sequentially. The interrelationship between VEGFR-2 and EGFR has been well established: VEGFR-2 signaling pathway inhibition enhances the anticancer activities of EGFR inhibitors, while the activation of VEGFR-2 is independent of EGFR signaling, which is blocked by EGFR inhibitors. Therefore, concurrent blocking of VEGFR-2 and EGFR signaling pathways appears to be a promising strategy in cancer treatment.[5,6]

VEGFR-2 inhibitors can be categorized into three types. Type I inhibitors occupy the ATP-binding region, forming a hydrogen bond with the hinge region amino acid Cys919. Type II inhibitors occupy the ATP binding site and extend over the gate area into the adjacent allosteric hydrophobic back pocket. Type III inhibitors block the receptor through hydrophobic interactions, and they accommodate the allosteric hydrophobic back pocket of VEGFR-2. Type II inhibitors are preferred over type I inhibitors due to their high affinity and selectivity. Moreover, type II inhibitors exhibit an increased drug-target residence time, resulting in prolonged TK suppression.[7] Therefore, diverse strategies have been employed to develop novel type II VEGFR-2 inhibitors (Fig. 1A).

Moreover, the ATP-binding pocket of EGFR-TK consists of five main regions. (a) Adenine binding pocket contains key amino acids, which can form hydrogen bonds with the adenine ring; (b) sugar region (hydrophilic ribose pocket); (c) hydrophobic region I plays an important role in inhibitor selectivity; (d) hydrophobic region II may be exploited for inhibitor specificity; (e) phosphate binding region can be used for improving inhibitor pharmacokinetics (Fig. 1B).[8]

N-heterocyclic compounds are essential building blocks of RNA and DNA and exert a significant role in the biochemical processes of living organisms.[9,10] They are recognizable scaffolds in drug discovery due to their biostability, structural variability and ability to form H bonds with biomolecules. Approximately 60% of FDA-approved small-molecule drugs include N-heterocyclic rings, emphasizing their importance in medicinal chemistry. Among them, pyrazole derivatives appear to provide specific value due to their extensive therapeutic potential, particularly in anti-cancer agent development.[9,11]

Pyrazole is an attractive choice as a substrate for the synthesis of several broad-spectrum biologically active pharmaceutical drugs. Globally, there are more than 50 pyrazole-based synthetic medicines on the market. These pyrazole-based marketed drugs target a varied range of clinical disorders, including rheumatoid arthritis, cystic fibrosis, sickle cell disease, non-small cell lung cancer (NSCLC), and hereditary angioedema.[12] Furthermore, a variety of pyrazole-based compounds have been recognized in cancer treatments as dual inhibitors of EGFR and VEGFR-2.[13,14]

Moreover, numerous drugs featuring pyrimidines (N-heterocycles) as the principal structural scaffold were recently FDA-approved as potential medications for a variety of cancer-related disorders. Most of these compounds inhibit VEGFR-2 and EGFR, which are vital receptor tyrosine kinases associated with the tumor microenvironment, to prevent tumor growth.[15]

Azobenzenes, which contain the N=N bond, have been reported as a multi-targeted scaffold in medicinal chemistry.[16] It has a variety of uses, including as antimicrobial, anti-inflammatory, antiviral, antidiabetic, anti-tuberculosis and anti-tumor agents.[17] Several *in vitro* and *in vivo* studies have confirmed that azo compounds could potentially act as anti-cancer agents. Giampietro *et al.* reported the synthesis, biological evaluation, and docking studies of a series of phenyldiazenyl sulfonamide compounds as aromatase inhibitors.[18] Moreover, Bustos *et al.* synthesized a series of 12 phenyldiazenyl pyrazoles and tested them against a wide library of cancer cell lines, including leukemia, colon, and brain cancer, showing that the compounds have anticancer activity.[19]

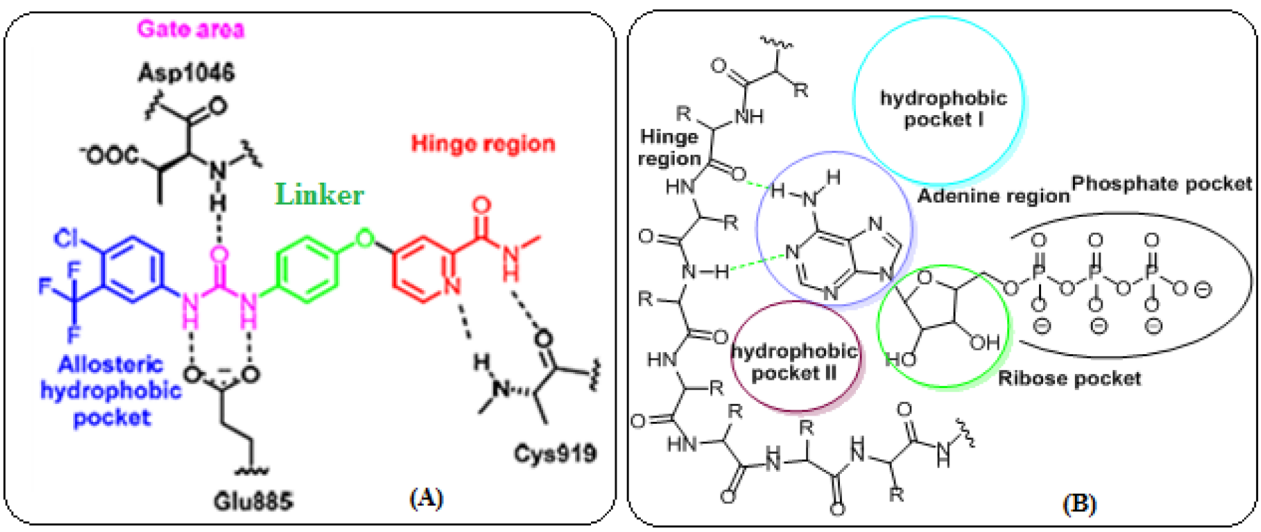

Fig. 1 (A) VEGFR-2 active site and (B) EGFR-TK active site.

All compounds showed a certain degree of growth inhibition against different cell lines. Highly selective growth inhibition activity was observed against the lung cancer, kidney cancer and leukemia cell lines. With the aim of identifying new anti-breast cancer compounds, Gomha *et al.* synthesized a series of thiazole-benzofuran phenyldiazenyl compounds. These molecules were evaluated for their anticancer activity against the human breast carcinoma (MCF-7) cell lines, compared with the doxorubicin drug.[20] In 2024, Tang *et al.* synthesized different azobenzene coumarin derivatives, where the coumarin moiety was linked to substituted phenyl and pyridine groups *via* amide bonds. These derivatives showed different degrees of anticancer activities against HeLa, A549, MCF-7, and HepG-2 cell lines.[21] Additionally, some azobenzene derivatives have been reported to show anti-pancreatic cancer activity.[22]

In 2024, Sandor and colleagues introduced a set of quinazoline–thiazole hybrid compounds with diazene spacers as potential antiproliferative and anti-angiogenic agents. The majority of these compounds exhibited enhanced antiproliferative activity (IC_{50} = 1.83–4.24 μM) against HepG2 cells compared to sorafenib (IC_{50} = 6.28 μM). The interaction with the VEGFR-2 kinase domain was evaluated using computational methods, such as molecular docking and molecular dynamics simulations. The compound series demonstrated a notable resemblance to sorafenib in terms of binding orientation within the VEGFR-2 active site, with compound **I** (Fig. 2) forming the most stable complex with VEGFR-2, in comparison to sorafenib. The highest free energy was observed for **I** (−71.23 ± 5.29 kcal mol^{-1}), which closely approximated the value for sorafenib (−69.39 ± 3.63 kcal mol^{-1}).[23]

In 2020, Srour and colleagues created another set of compounds based on a combination of benzimidazole and thiazole with the diazene moiety to act as EGFR inhibitors. Compound **II** (Fig. 2) exhibited notable efficacy as an EGFR tyrosine kinase inhibitor and achieved anti-breast cancer treatment, with IC_{50} values of 109.71 ± 3.55 nM and 6.30 ± 0.37 μM, respectively.[24]

Kinase inhibitors have significant therapeutic potential in oncology, as they specifically target abnormal kinases responsible for the malignancy of cancer cells. By disturbing the signaling pathways that cancer cells rely on to divide and survive, these inhibitors can efficiently prevent tumor growth.[25]

Certain kinase inhibitors have been designed to target receptor tyrosine kinases (RTKs), which are often mutated or overexpressed in cancers, such as breast, lung and colorectal cancers.[26] Among the many classes of kinase inhibitors, pyrazoles[27] and pyrimidines[28] have received considerable attention due to their potent inhibition of kinases closely associated with cancer and other diseases.

These products bind to the ATP-binding site of kinases, thereby preventing the transfer of phosphate required for the signal transduction pathways of cancer cell survival and proliferation.[29] Moreover, various pyrimidines and pyrazoles have been designated as EGFR and VEGFR-2 inhibitors.[30] Furthermore, numerous phenyldiazene-containing compounds have been described as anticancer agents that inhibit both VEGFR-2 and $EGFR^{T790M}$ receptors.[31]

Based on former findings and as an extension of our research program in developing and synthesizing various anticancer derivatives,[32–36] new pyrazoles and pyrimidines containing azobenzenes were prepared and assessed for cytotoxicity against HepG2, A549, MCF-7 and HCT-116 cell lines.

The selectivity of the active compounds was also evaluated on normal human MCF-10 cell lines. Additionally, all compounds were assessed for both $EGFR^{T790M}$ and VEGFR-2 inhibition. Docking experiments were also conducted in the $EGFR^{T790M}$ and VEGFR-2 active sites to predict their probable binding modes and orientations.

2. Structure-based and rationale design

New pyrazoles and pyrimidines substituted with azobenzenes were designed and synthesized according to the structural requirements for both VEGFR-2 and $EGFR^{T790M}$ inhibition.

The new derivatives were obtained through bioisosteric modification of VEGFR-2 inhibitors (sorafenib and pazopanib) at four different parts.[37–39] The hydrophobic substituted phenyl tails of sorafenib and pazopanib that occupy the hydrophobic pocket were replaced by unsubstituted phenyl groups. The hydrogen bond donor (HBD) urea and/or amino spacers were replaced by HBA diazene (N═N) groups that can bind to Glu885 and/or Asp1046. The central hydrophobic phenoxy and/or *N*-methylpyrimidine linkers of sorafenib and pazopanib, respectively, were replaced by azobenzene moieties. The substituted hetero-aromatic systems, specifically the *N*-methylpicolinamide and/or the 2,3-dimethyl-2*H*-indazol-6-yl moieties of sorafenib

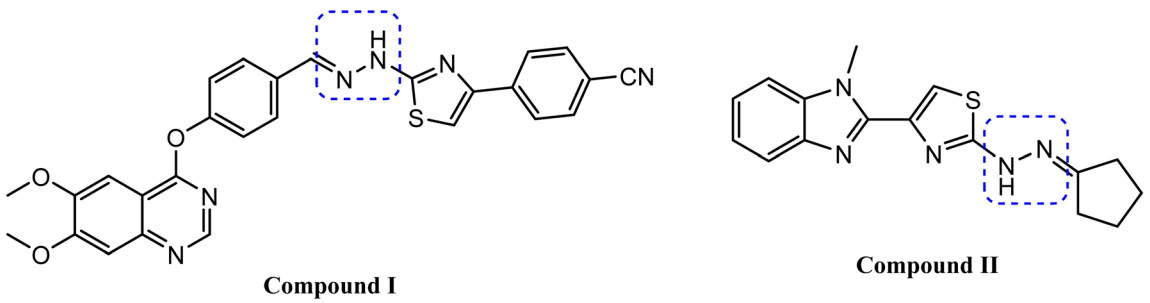

Fig. 2 Reported compounds with the diazene moiety as VEGFR-2 and EGFR-TK inhibitors.

and pazopanib, respectively, were replaced by substituted pyrazoles **3–8** and/or pyrimidines **9–12**, respectively (Fig. 3).

In the same manner, our new derivatives were obtained through modifications of the EGFR inhibitors (erlotinib and gefitinib) at four positions.[40,41] The hydrophobic bis(2-methoxyethoxy) and 3-morpholinopropoxy tails of erlotinib and gefitinib, respectively, that occupy the hydrophobic region II were replaced by the terminal hydrophobic azobenzene moieties. The HBD NH group was replaced by the NH_2 group. The hetero-aromatic quinazoline scaffold that occupies the adenine pocket was replaced by the hetero-aromatic pyrazole and/or pyrimidine rings linked to azobenzenes. The lipophilic 3-ethynylphenyl and 3-chloro-4-fluorophenyl heads of erlotinib and gefitinib, respectively, that occupy hydrophobic region I

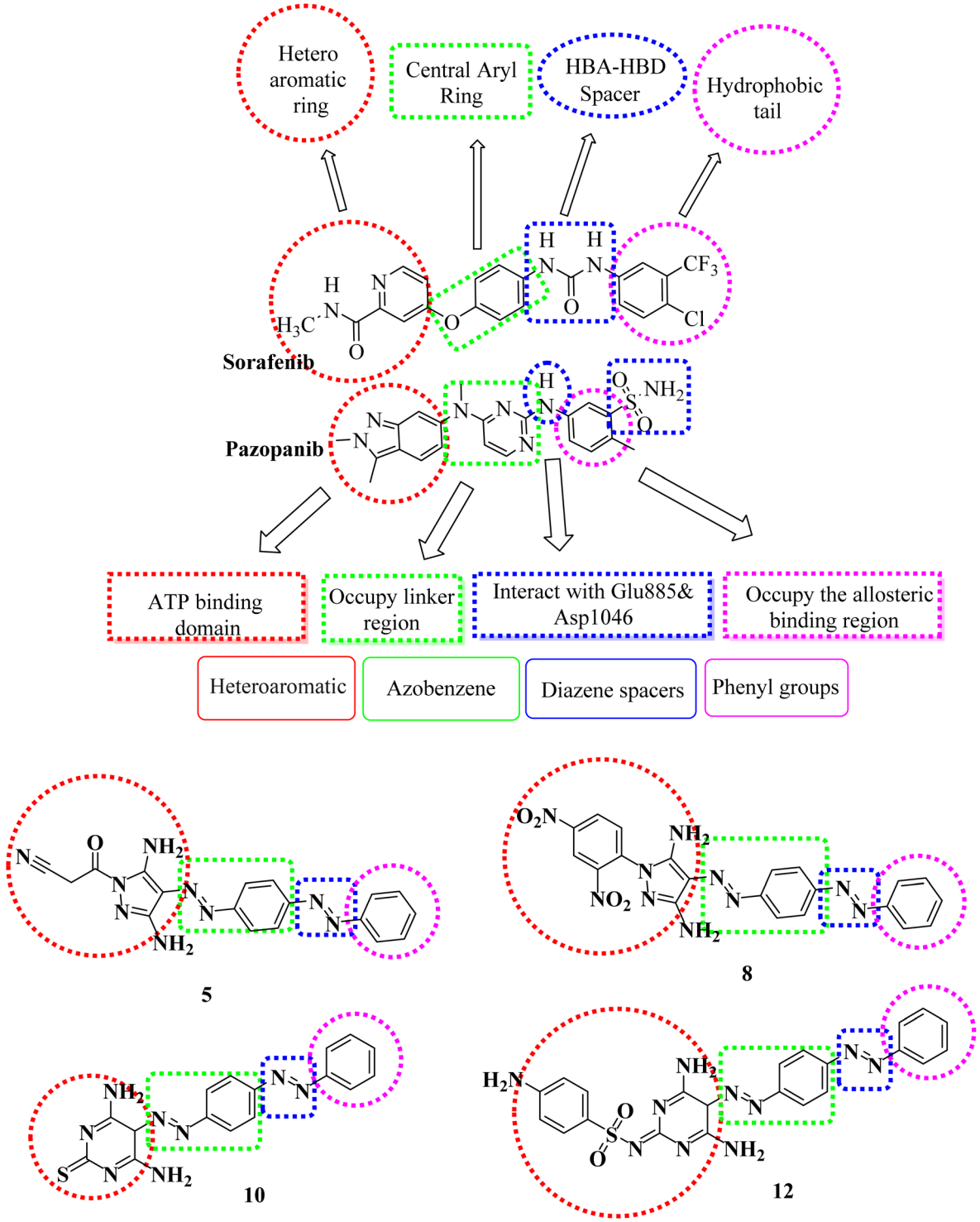

Fig. 3 Pharmacophoric and structural similarities of some designed compounds and VEGFR-2 inhibitors.

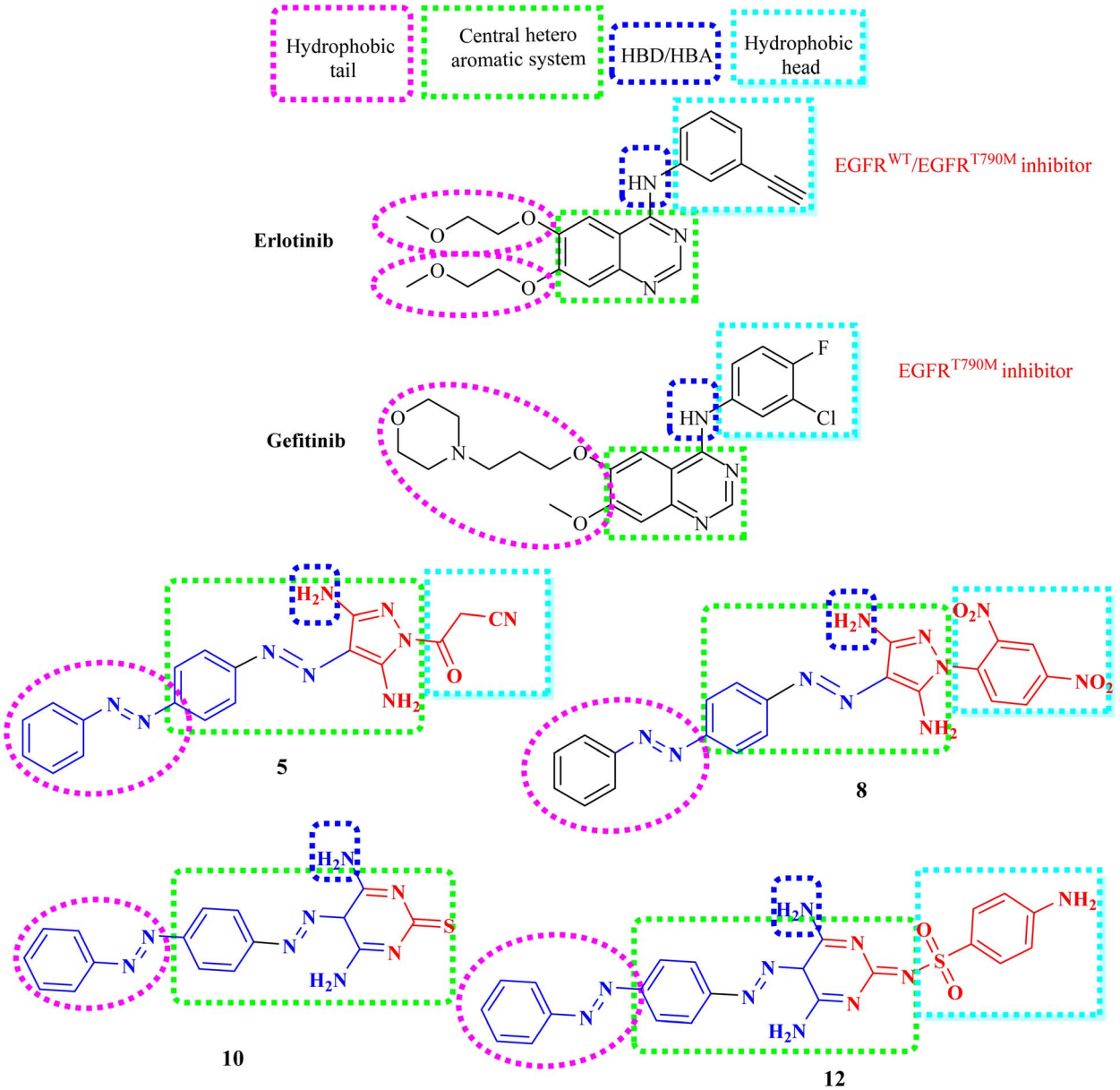

Fig. 4 Design rationale based on the structural characteristics of EGFR inhibitors.

were replaced by different aliphatic and/or aromatic groups (Fig. 4).

3. Results and discussion

3.1. Chemistry

Our derivatives were synthesized following the reactions described in Schemes 1–3. The reaction of 4-(phenyldiazenyl) aniline with $NaNO_2$ in the presence of HCl at 0–5 °C gives the diazonium chloride salt **1**, which couples with malononitrile to yield the key compound 2-(4-(phenyldiazenyl)phenyldiazenyl)-malononitrile (**2**) (Scheme 1) according to the described technique.[42–44]

Derivative **2** was cyclized with the appropriate thiosemicarbazide, semicarbazide, 2-cyanoacetohydrazide, acetohydrazide, phenyl hydrazine, or 2,4-dinitrophenyl hydrazine (DNP) in acetone at reflux temperature for 5–30 h to give the corresponding targeted pyrazole derivatives **3–8** (Scheme 2). The structure of compound **5** produced IR absorption bands at 3443 (NH_2), 2194 (CN) and 1657 (C=O). The ^{1}H NMR spectrum of compound **5** showed one singlet signal for CH_2 at 2.41. Additionally, two D_2O exchangeable singlet signals were observed for the $2NH_2$ groups at 5.86 and 6.30. Moreover, the ^{13}C-NMR data support the structure.

Derivative **2** was used to synthesize the novel pyrimidines (**9–12**) through cyclization reactions with the suitable urea, thiourea, guanidine and/or sulfaguanidine in DMF using a water bath for 8–12 h to obtain the corresponding products **9–12** (Scheme 3).

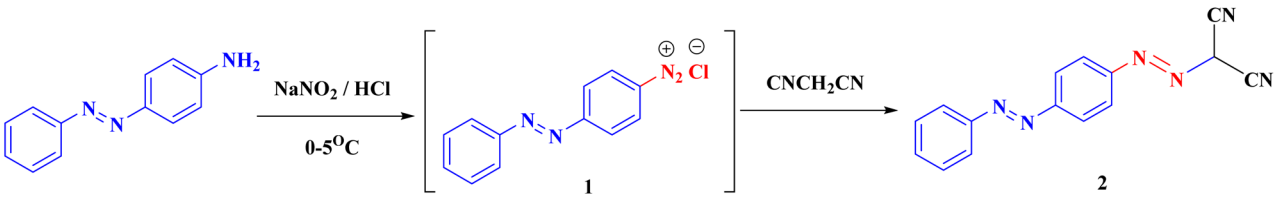

Scheme 1 Synthesis of compound 2.

3.2. Microwave and conventional techniques assessment

A comparative evaluation between microwave-assisted and conventional methods was conducted using several green chemistry efficiency parameters, including yield economy (YE), atomic economy (AE), reaction mass efficiency (RME), and optimum efficiency (OE). The reaction times and yields obtained for both methods were compared[45–49] (Table 1).

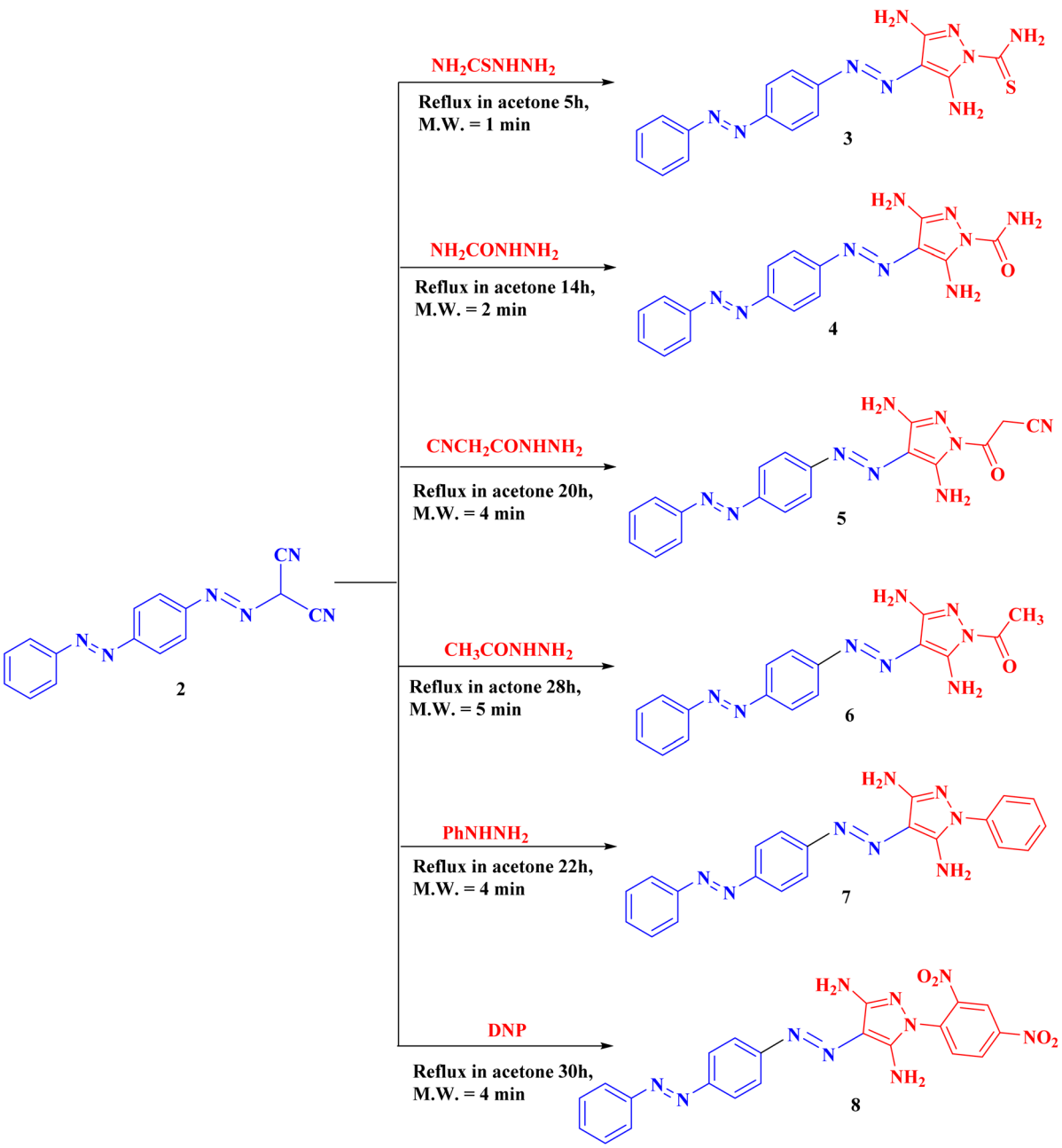

Scheme 2 Syntheses of the targeted compounds 3–8.

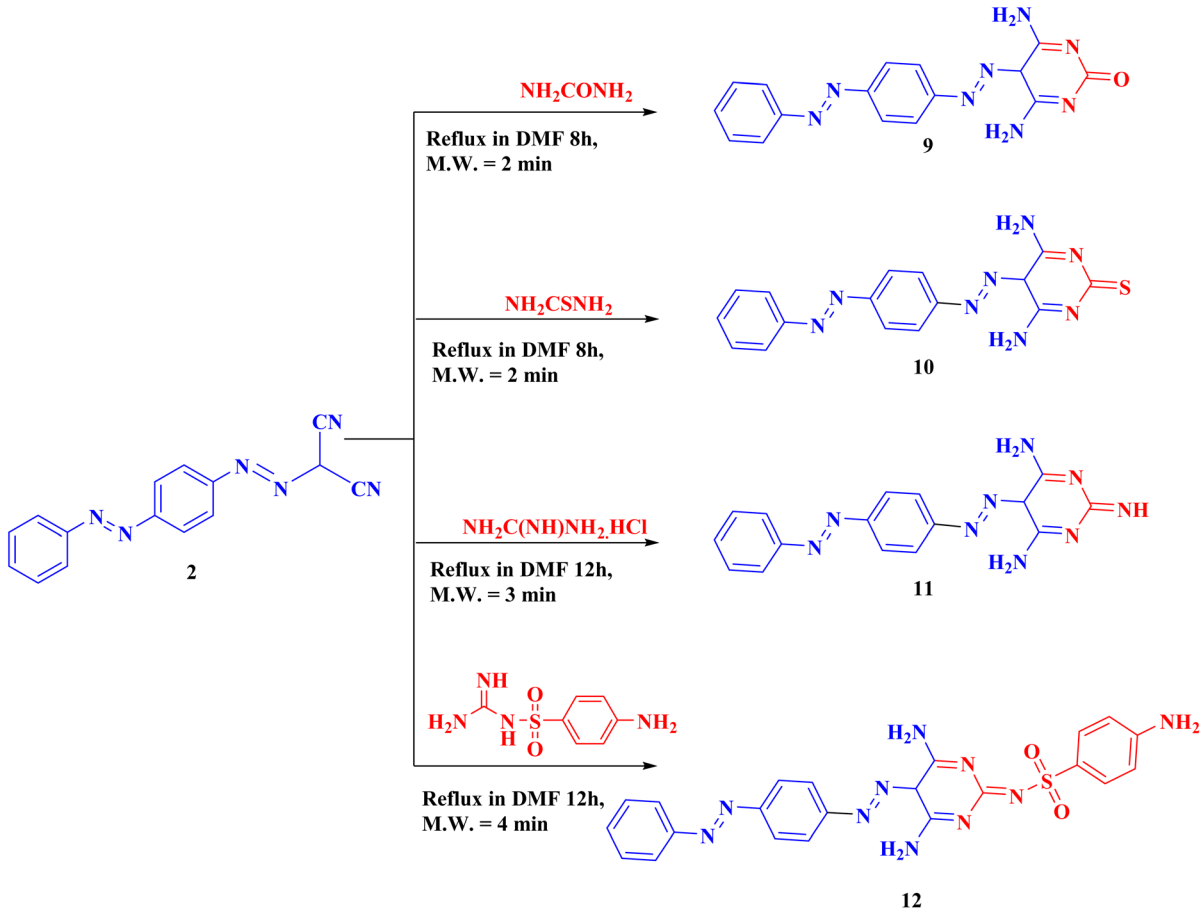

Scheme 3 Syntheses of compounds 9–12.

The yield economy (YE) was employed to identify the most efficient method for reaction accomplishment and was calculated according to the following equation:

$$\text{YE} = \text{yield (\%)/time (min)}$$

The reaction mass efficiency (RME) was calculated using the equation:

$$\text{RME} = \text{(weight of isolated product)/(total weight of reactants)}$$

In addition, the optimum efficiency (OE) was employed as a comparative parameter between the two methods and was calculated as follows:

$$\text{OE} = (\text{RME/AE}) \times 100$$

Table 1 Comparative study of the microwave and conventional techniques

	Time "min"		Yield (%)		YE		OE		RME		
Compound no.	M.W.[b]	Conv.[a]	M.W.	Conv.	M.W.	Conv.	M.W.	Conv.	M.W.	Conv.	AE
3	1	300	90	54	90.00	0.1800	0.7766	0.3883	77.66	38.83	100
4	2	840	92	51	46.00	0.0607	0.7996	0.4431	72.48	40.17	90.65
5	4	1200	91	53	22.75	0.0442	0.7875	0.4587	78.75	45.87	100
6	5	1680	90	52	18.00	0.0310	0.7714	0.4457	77.14	44.57	100
7	4	1320	90	52	22.50	0.0394	0.7814	0.4515	78.14	45.15	100
8	4	1800	92	53	23.00	0.0294	0.8193	0.4720	81.93	47.20	100
9	2	480	90	54	45.00	0.1125	0.7386	0.4431	73.86	44.31	100
10	2	480	92	52	46.00	0.1083	0.7612	0.4303	76.12	43.03	100
11	3	720	90	51	30.00	0.0708	0.7514	0.4258	67.81	38.42	90.24
12	4	720	91	51	22.75	0.0708	0.7916	0.4436	79.16	44.36	100

[a] Conv.: conventional technique. [b] M.W.: microwave irradiation technique.

Table 2 ΔG in kcal mol^{-1} for the VEGFR-2 binding ligands

Compound	ΔG [kcal mol^{-1}]	Compound	ΔG [kcal mol^{-1}]
3	−75.00	**9**	−81.91
4	−68.21	**10**	−90.88
5	−83.99	**11**	−79.79
6	−80.36	**12**	−106.48
7	−79.91	Sorafenib	−99.50
8	−91.33		

While atomic economy (AE) represents the theoretical maximum efficiency of a reaction, RME reflects the actual mass efficiency. The AE values for both the microwave and conventional methods are identical, as the same target molecules were synthesized from identical reactants under different reaction conditions, as shown in Table 1.

3.3. Docking studies

The Molsoft program was used to assess the binding affinities and orientations of our derivatives inside the active sites of both VEGFR-2 (PDB ID: 4ASD)[50,51] and EGFR^{T790M} (PDB ID: 3W2O).[44,52]

3.3.1. As VEGFR-2 inhibitors. Our derivatives showed identical orientations in the binding site of VEGFR-2 and displayed very good affinities (Table 2).

Sorafenib presented −99.50 kcal mol^{-1} and formed five H bonds with Cysteine919 (2.51 Å and 2.10 Å), Glutamate885 (2.75 Å and 1.77 Å) and Aspartate1046 (1.50 Å). The 3-trifluoromethyl-4-chlorophenyl tail inhibited the hydrophobic pocket constructed by Isoleucine892, Isoleucine888, Histidine1026, Glutamate885, Aspartate1046 and Cysteine1045. Moreover, the substituted hetero-aromatic pyridine ring inhibited the pocket formed by Cysteine919, Phenylalanine918, Glutamate917, Valine848, Lysine920, Leucine1035, and Leucine840. Furthermore, the central phenoxy linker inhibited the hydrophobic pocket formed by Leucine1035, Cysteine1045, Valine848, and Lysine868 (Fig. 5).

Compound **12** exhibited −106.48 kcal mol^{-1} and formed 6H bonds with Cys919 (2.53 Å), Glu917 (1.61 Å and 2.42 Å), Asp1046 (1.97 Å), Asn923 (2.57 Å) and Leu840 (2.49 Å). The distal phenyldiazene tail inhibited the hydrophobic domain formed by Ile1025, Ile888, Asp1046, Hie1026, Glu885, Cys1045 and Ile892. Moreover, the aromatic 4-aminophenyl ring inhibited the pocket formed by Cys919, Lys920, Leu1035, Phe918, Asn923, and Leu840. Furthermore, the central azobenzene linker inhibited the pocket formed by Cys1045, Val848, Lys868, Glu917 and Asp1046 (Fig. 6).

In the same manner, compound **8** showed nearly the same binding orientation as **12**, with −91.33 kcal mol^{-1}, and it formed 7 hydrogen bonds with Asp1046 (2.08 Å and 2.34 Å), Cys919 (1.66 Å and 2.38 Å), Gly922 (2.44 Å) and Glu917 (1.72 Å and 2.30 Å) (Fig. 7).

Similarly, derivative **10** showed nearly the same orientation as **12**, with −90.88 kcal mol^{-1}, and it formed 4H bonds with Asp1046 (1.69 Å and 2.72 Å), Cys919 (1.97 Å) and Glu917 (1.68 Å) (Fig. 8).

3.3.2. As EGFR^{T790M} inhibitors. Our derivatives also showed identical orientations in the binding site of EGFR^{T790M} and exhibited very good affinities (Table 3).

Erlotinib displayed −82.77 kcal mol^{-1} and formed four H-bonds with Thr854 (2.99 Å), Cys797 (2.05 Å), Methionine793 (1.82 Å), and Valine726 (2.97 Å). The 3-ethynylphenyl head

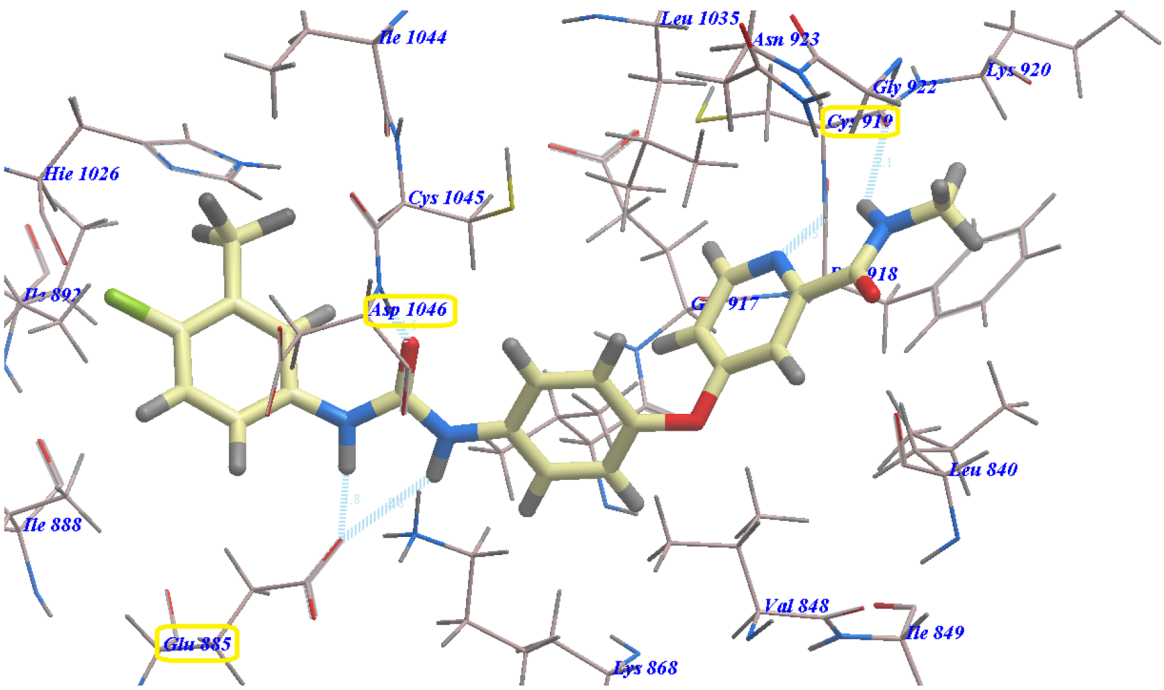

Fig. 5 Sorafenib orientation with VEGFR-2 binding.

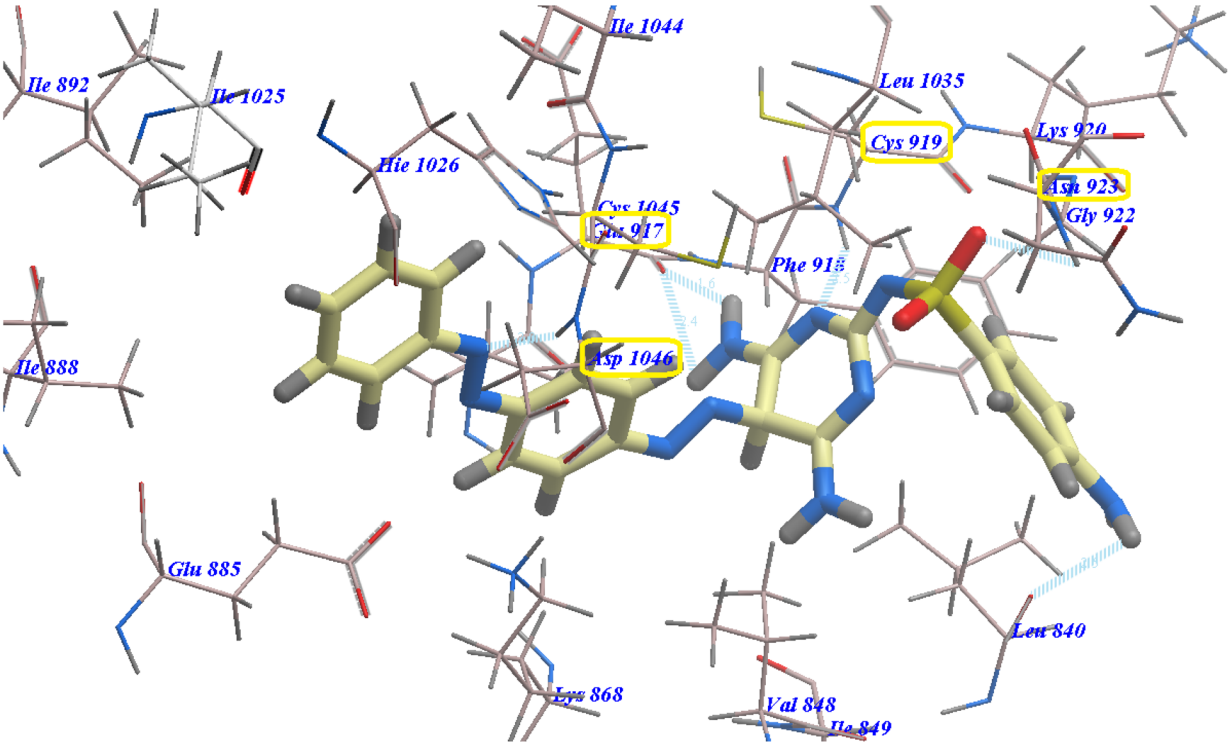

Fig. 6 Predicted binding mode of compound **12** with VEGFR-2.

inhibited the hydrophobic area I produced by Ile759, Phe723, Gly724, Asp855, Thr854, Val726, Glu762, Leu777, Met790 and Glu791. Similarly, the 2-methoxyethoxy end inhibited the hydrophobic groove II produced by Leu844, Met793, Leu718, Pro794 and Val845 (Fig. 9).

Derivative **12** showed −99.31 kcal mol^{-1} and formed 9H bonds with Met793 (2.98 Å), Glu762 (1.96 Å and 2.28 Å), Ala743 (2.76 Å and 2.96 Å), Lys745 (1.71 Å), Asp855 (2.26 Å and 2.95 Å) and Thr854 (2.99 Å). The azobenzene side chain inhibited the hydrophobic area II produced by Pro794, Met793, Leu718,

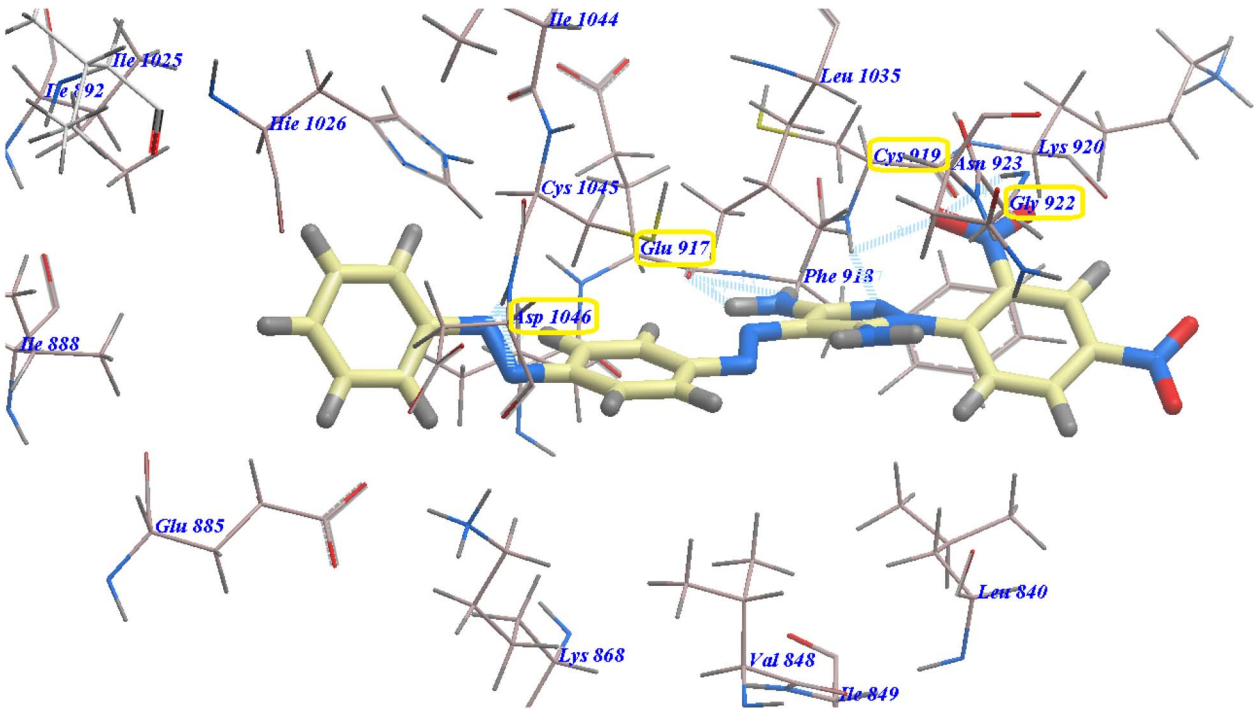

Fig. 7 Expected binding mode of compound **8** with VEGFR-2.

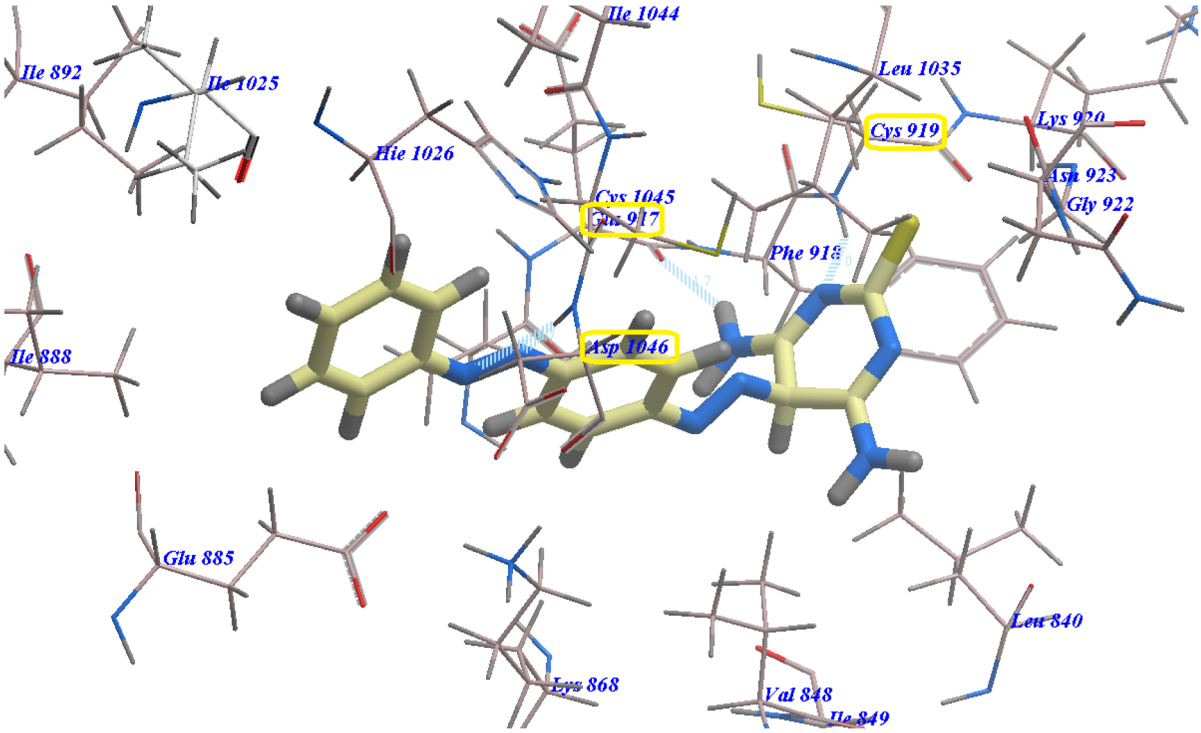

Fig. 8 Expected binding mode of compound **10** with VEGFR-2.

Val726, Val845, Glu791, Met790, Ala743 and Leu844. Moreover, the sulfonylaniline head inhibited the hydrophobic area I formed by Gly724, Glu762, Asp855, Phe723, Ile759 and Thr854 (Fig. 10).

Also, derivative **8** exhibited nearly the same orientation as **12** (-80.68 kcal mol^{-1}). It formed 6H bonds with Met793 (2.95 Å), Lys745 (2.51 Å), Glu791 (2.13 Å and 2.38 Å), Asp855 (2.77 Å) and Thr854 (2.29 Å) (Fig. 11).

Derivative **10** displayed nearly the same orientation as **12**, with -79.46 kcal mol^{-1}, and it formed 5H bonds with Met793 (2.92 Å and 2.96 Å), Lys745 (2.98 Å), Glu791 (2.64 Å) and Thr854 (2.06 Å) (Fig. 12).

3.4. Biological testing

3.4.1. *In vitro* cytotoxicity assessment. The cytotoxicity of derivatives **3–12** was assessed against A549, MCF-7, HCT-116, and HepG2 cell lines using the MTT method.[53–55] A549, MCF-7, HCT-116, and HepG2 cells were obtained from the American Type Culture Collection (ATCC, Manassas, USA). The standard drugs, sorafenib and erlotinib, were used (Table 4). The HCT116 and A549 cell lines were highly sensitive to our derivatives. Compound **12** exhibited the highest potency against A549, HepG2, MCF-7, and HCT116 cancer cell lines, with IC_{50} = 5.12, 6.77, 5.85, and 5.25 μM, respectively. It presented higher cytotoxicity than erlotinib (IC_{50} = 5.49, 7.73, 8.20, and 13.91 μM, respectively) and showed lower cytotoxicity than sorafenib (IC_{50} = 4.04, 4.00, 5.58, and 5.05 μM, respectively).

Against the HCT116 cell lines, compounds **5**, **6**, **7**, **8**, **9** and **10**, with IC_{50} = 6.00–8.25 μM, offered very good cytotoxicity. Compound **11**, with IC_{50} = 10.25 μM, offered good cytotoxicity. Additionally, derivatives **3** and **4**, with IC_{50} = 15.75 and 18.30 μM, respectively, showed moderate cytotoxicity.

Against the MCF-7 cell lines, derivatives **5**, **6**, **7**, **8**, **9** and **10**, with IC_{50} = 7.15–8.60 μM, offered very good cytotoxicity. Compound **11**, with IC_{50} = 10.80 μM, offered good cytotoxicity. Additionally, derivatives **3** and **4**, with IC_{50} = 15.25 and 18.50 μM, respectively, showed moderate cytotoxicity.

With regard to the HepG2 cell lines, derivatives **5**, **6**, **8**, **9** and **11**, with IC_{50} = 7.85–9.75 μM, showed very good cytotoxicity. Compounds **7** and **10**, with IC_{50} = 10.25 and 11.90 μM, offered good cytotoxicity. Additionally, derivatives **3** and **4**, with IC_{50} = 15.90 and 19.60 μM, respectively, showed moderate cytotoxicity.

Against the A549 cell lines, compounds **5**, **6**, **7**, **8**, **9**, **10** and **11**, with IC_{50} = 6.10–8.80 μM, offered very good cytotoxicity. Additionally, derivatives **3** and **4**, with IC_{50} = 17.50 and 15.20 μM, respectively, showed moderate cytotoxicity.

Moreover, the cytotoxicity of the significantly potent derivatives **5**, **6**, **8**, **9**, **10** and **12** was evaluated against the MCF-10 healthy cell lines. The estimated structures indicated low toxicity against the MCF-10 cells, with IC_{50} = 50.90–55.50 μM. Compounds **5**, **6**, **8**, **9**, **10** and **12** exhibited 8.09-, 6.53-, 8.92-, 7.30-, 8.10- and 10.57-fold higher toxicity against HCT-116 cells, respectively, than against MCF-10 cells. Equivalently, derivatives **5**, **6**, **8**, **9**, **10** and **12** exhibited 7.28-, 6.44-, 7.48-, 7.17-, 7.16- and 9.49-fold higher toxicity against MCF-7 cells, respectively, than against healthy MCF-10 cells. In addition, derivatives **5**, **6**, **8**, **9**, **10** and **12** exhibited 6.94-, 5.22-, 7.28-, 6.57-, 6.84- and 8.20-fold higher toxicity against HepG2 cells, respectively, than against MCF-10 cells. Also, derivatives **5**, **6**, **8**, **9**, **10** and **12** displayed 7.64-, 6.74-, 8.77-, 7.22-, 7.58- and 10.84-fold higher

Table 3 Ligands ΔG (kcal mol^{-1}) for binding with EGFR^{T790M}

Compound	ΔG [kcal mol^{-1}]	Compound	ΔG [kcal mol^{-1}]
3	−57.55	**9**	−76.16
4	−64.31	**10**	−79.46
5	−77.54	**11**	−72.40
6	−72.04	**12**	−99.31
7	−67.67	Erlotinib	−82.77
8	−80.68		

toxicity against A549 cells, respectively, than against MCF-10 cells.

Statistical comparisons relative to sorafenib and erlotinib were performed using pairwise Welch's *t*-tests (assuming $n = 3$). The compounds exhibited a broad range of cytotoxic activities, with IC_{50} values spanning 5.12–19.60 μM. Compounds **3** and **4** were the least potent derivatives, displaying IC_{50} values generally exceeding 15 μM across all tested cell lines. In contrast, compounds **7**, **9**, and **11** demonstrated moderate activities, particularly against HCT-116 and MCF-7 cells, with IC_{50} values in the range of 7.25–10.80 μM. Notably, compounds **5** and **6** showed enhanced cytotoxicity toward HepG2 cells ($IC_{50} = 7.93 \pm 0.8$ and 9.75 ± 1.0 μM, respectively), and their activity was statistically comparable to that of erlotinib ($p > 0.05$), indicating potentially relevant efficacy in hepatocellular carcinoma models. Among the evaluated derivatives, compound **12** emerged as the most potent analogue, exhibiting consistently low IC_{50} values across all cancer cell lines (5.12–6.77 μM). Statistical analysis revealed that its antiproliferative activities against HCT-116 and MCF-7 cells were statistically indistinguishable from those of sorafenib ($p > 0.05$), indicating comparable potency to the clinically used multikinase inhibitor. Moreover, compound **12** demonstrated significantly greater potency than erlotinib in these cell lines ($p < 0.01$), supporting its superior cellular efficacy. Compounds **8** and **10** displayed notable cytotoxic activity, particularly against HCT-116 cells ($IC_{50} = 6.00 \pm 0.5$ and 6.50 ± 0.5 μM, respectively), where both were significantly more potent than erlotinib ($p < 0.01$). Their activity was statistically comparable to that of sorafenib in selected assays ($p > 0.05$), supporting their clinically relevant potency, although their overall antiproliferative effects remained slightly weaker than those of compound **12**. These findings position compounds **8** and **10** as promising secondary leads. To gain mechanistic insights, the compounds were evaluated for their inhibitory activity against VEGFR-2 and the resistant EGFR^{T790M} kinase. In the EGFR^{T790M} assay, compound **12** exhibited inhibitory potency statistically comparable to that of erlotinib ($p > 0.05$), confirming the effective inhibition of the clinically relevant resistance mutation. Compounds **8** and **10** also demonstrated low micromolar inhibitory activities, with potencies statistically comparable to that of erlotinib in this assay, albeit with slightly higher IC_{50} values. In the VEGFR-2 inhibition assay, compound **12** again showed the strongest

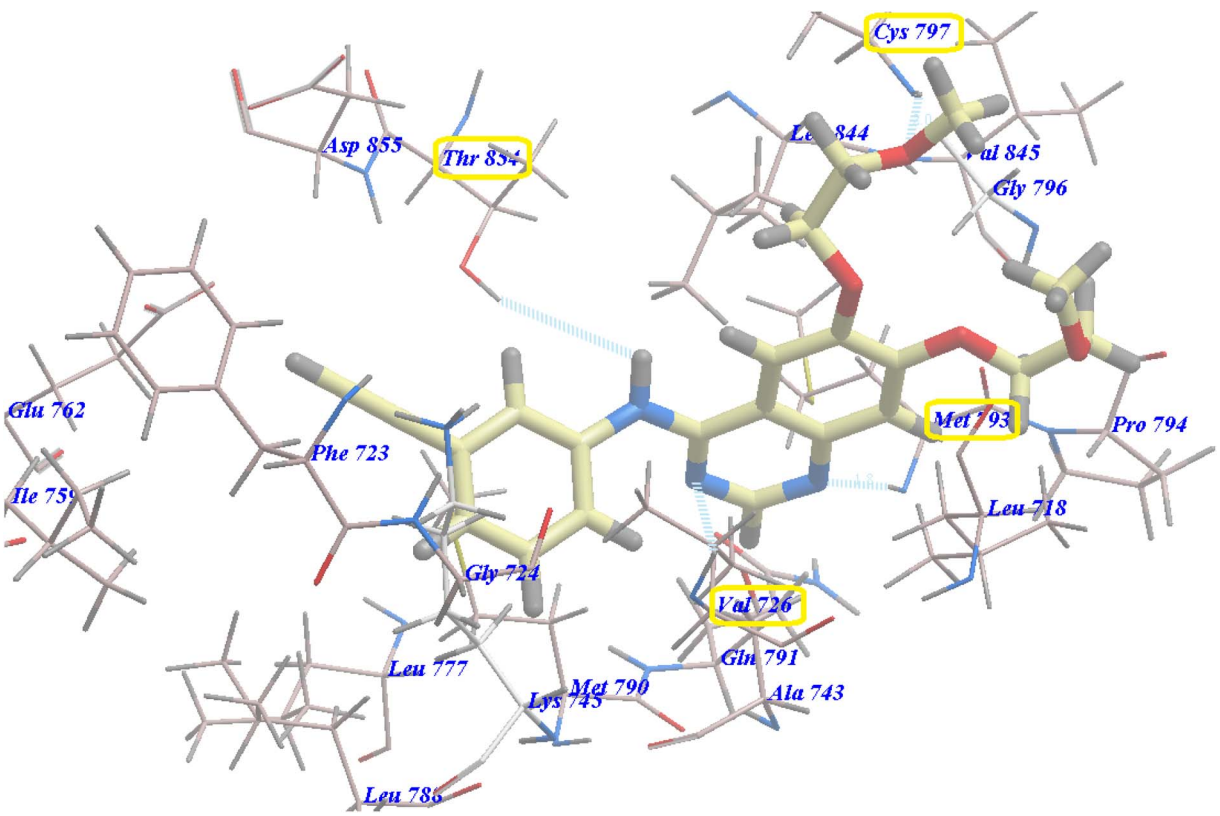

Fig. 9 Expected binding mode of erlotinib with EGFR^{T790M}.

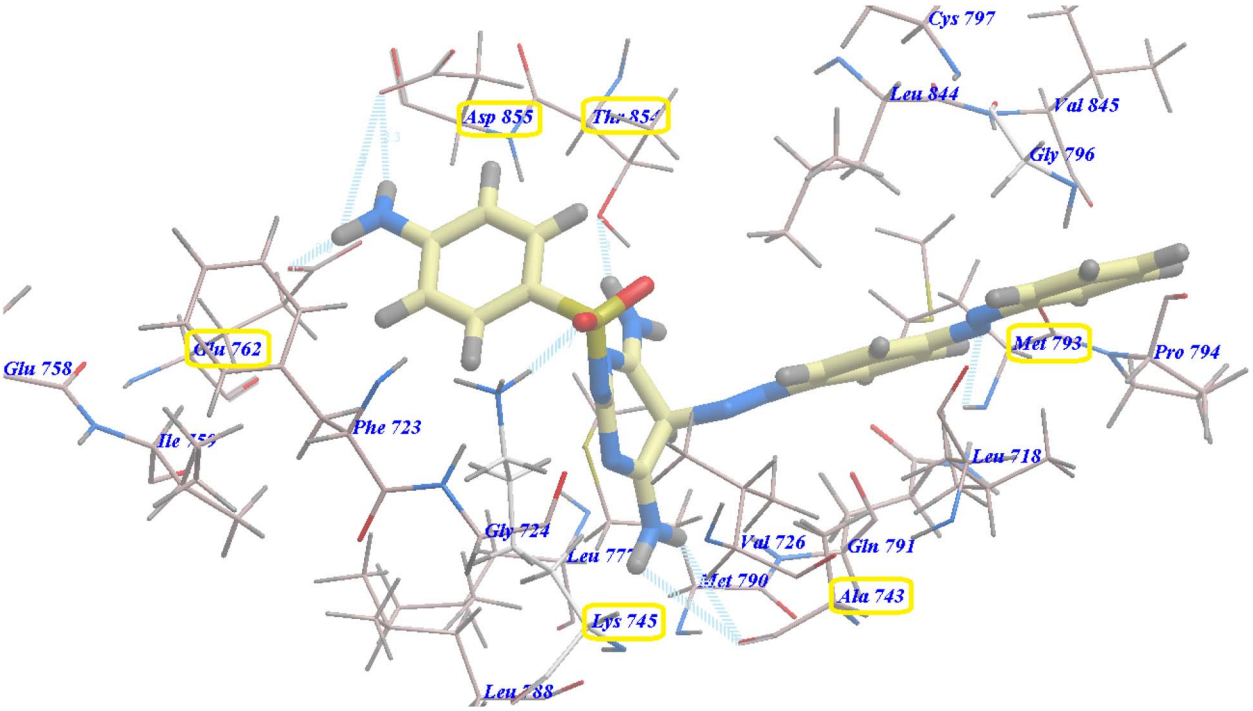

Fig. 10 Expected binding mode of derivative **12** with EGFR^{T790M}.

activity ($IC_{50} = 0.90 \pm 0.15$ μM), with no statistically significant difference relative to sorafenib ($p > 0.05$), indicating comparable anti-angiogenic potential. Compounds **8** and **10** displayed measurable VEGFR-2 inhibition, with IC_{50} values close to that of sorafenib, and no statistically significant differences, supporting partial dual-target engagement, although their inhibitory profiles were less consistent than that of compound **12**. Overall, the combined cellular and biochemical data identify compound **12** as the most advanced lead candidate, characterized by high antiproliferative potency, favorable selectivity toward cancer cells, and dual inhibition of VEGFR-2 and EGFR^{T790M} with activity statistically comparable to those of established

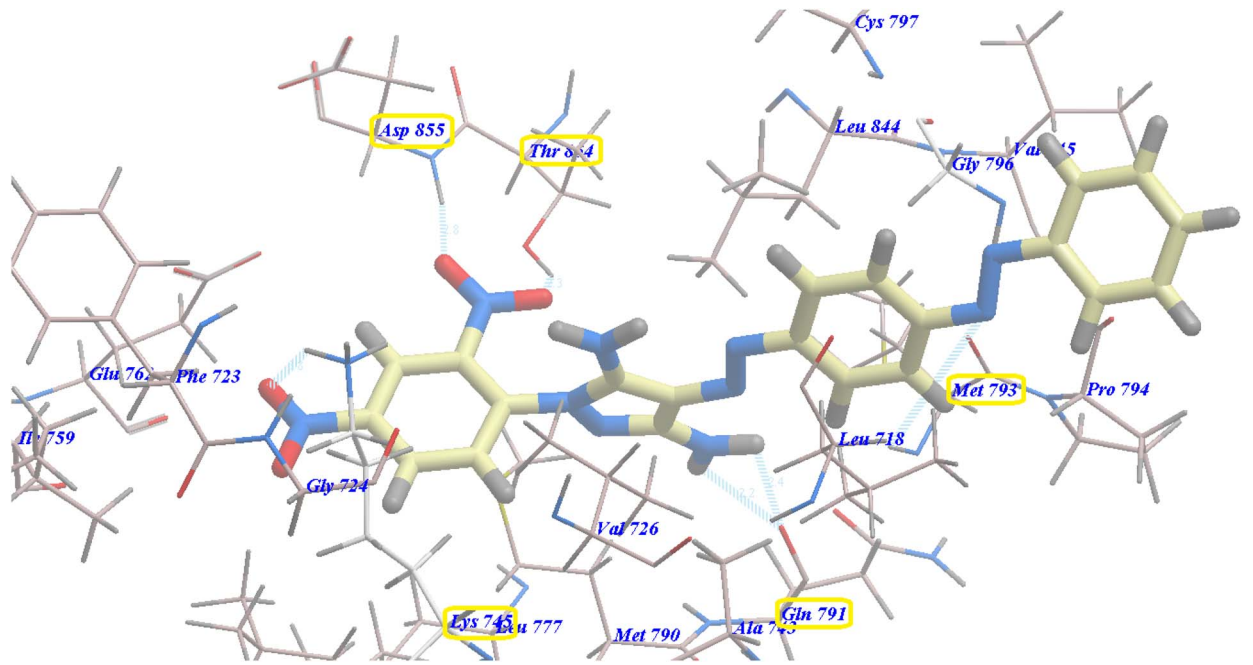

Fig. 11 Expected binding mode of compound **8** with EGFR^{T790M}.

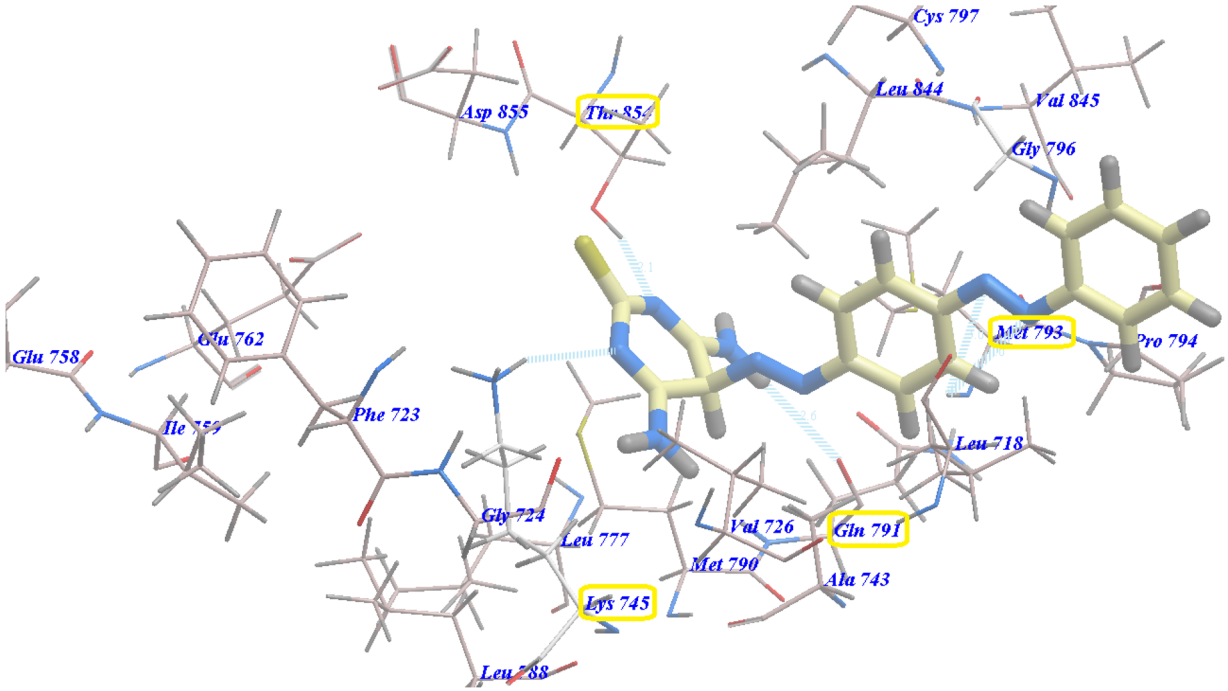

Fig. 12 Expected binding mode of compound **10** with EGFR^{T790M}.

reference drugs. Compounds **8** and **10** represent promising secondary scaffolds, exhibiting clinically relevant cytotoxicity and kinase inhibition in selected assays.

3.4.2. VEGFR-2 kinase inhibitory assay. The VEGFR-2 inhibition activity of our compounds was assessed using an anti-phosphotyrosine antibody with the Alpha Screen system (PerkinElmer, USA).[56] All compounds displayed strong-to-low inhibitions, with IC_{50} = 0.90–2.45 μM (Table 4). Compounds **12**, **8** and **10** exhibited very good VEGFR-2 inhibitions, with IC_{50} = 0.90, 0.95 and 1.00 μM, respectively. Compounds **5**, **6** and **9** displayed good inhibitions, with IC_{50} = 1.30, 1.08 and 1.12 μM, respectively. Also, structures **7** and **11** gave moderate inhibitions, with IC_{50} = 1.50 and 1.70 μM, respectively. Also, structures **3** and **4** showed lower inhibitions, with IC_{50} = 2.20 and 2.45 μM, respectively.

3.4.3. EGFR^{T790M} kinase inhibitory assay. EGFR^{T790M} inhibition was evaluated for our derivatives using HTRF (homogeneous time resolved fluorescence).[57] EGFR overexpression has been associated with metastasis, a poor prognosis and high violence in a number of cancers.[58] Erlotinib, with IC_{50} = 0.24 μM, was used as the reference drug (Table 4).

All compounds displayed strong-to-low inhibitions, with IC_{50} = 0.90–2.45 μM (Table 4). Compounds **12**, **8**, **10**, **5** and **9** showed strong EGFR^{T790M} inhibitions, with IC_{50} = 0.25, 0.30, 0.33, 0.35

Table 4 *In vitro* anticancer effects of our compounds on the A549, HepG2, HCT-116, MCF-7 and MCF-10 cell lines and VEGFR-2/EGFR^{T790M} kinases assays

	IC_{50}[a] (μM)						
Comp.	HCT116	MCF-7	HepG2	A549	MCF-10	VEGFR-2	EGFR^{T790M}
3	15.75 ± 1.5	15.25 ± 1.5	15.90 ± 1.5	17.50 ± 1.5	NT[b]	2.20 ± 0.50	1.60 ± 0.15
4	18.30 ± 1.5	18.50 ± 1.5	19.60 ± 1.5	15.20 ± 5.5	NT[b]	2.45 ± 0.15	1.45 ± 0.25
5	7.80 ± 0.5	7.90 ± 0.5	7.93 ± 0.8	7.20 ± 0.5	55.00 ± 2.9	1.30 ± 0.15	0.35 ± 0.15
6	6.80 ± 0.5	7.55 ± 0.5	9.75 ± 1.0	7.55 ± 0.5	50.90 ± 2.9	1.08 ± 0.15	0.54 ± 0.15
7	8.25 ± 0.5	8.60 ± 0.5	10.25 ± 1.5	8.80 ± 0.8	NT[b]	1.50 ± 0.15	0.62 ± 0.15
8	6.00 ± 0.5	7.15 ± 0.5	7.35 ± 0.5	6.10 ± 0.5	53.50 ± 2.9	0.95 ± 0.15	0.30 ± 0.15
9	7.25 ± 0.5	7.38 ± 0.5	8.06 ± 0.5	6.95 ± 0.5	52.95 ± 2.9	1.12 ± 0.50	0.40 ± 0.15
10	6.50 ± 0.5	7.35 ± 0.5	11.90 ± 1.1	7.50 ± 0.5	52.66 ± 2.9	1.00 ± 0.15	0.33 ± 0.15
11	10.25 ± 1.1	10.80 ± 1.0	7.70 ± 0.5	7.33 ± 0.5	NT[b]	1.70 ± 0.50	0.50 ± 0.25
12	5.25 ± 0.5	5.85 ± 0.5	6.77 ± 1.1	5.12 ± 0.5	55.50 ± 2.9	0.90 ± 0.15	0.25 ± 0.15
Sorafenib	5.05 ± 0.50	5.58 ± 0.55	4.00 ± 0.33	4.04 ± 0.33	NT[b]	0.84 ± 0.04	NT[b]
Erlotinib	13.91 ± 1.3	8.20 ± 0.34	7.73 ± 0.67	5.49 ± 0.45	NT[b]	NT[b]	0.24 ± 0.22

[a] IC_{50} values are the mean ± S.D. of three separate experiments. [b] NT = not tested.

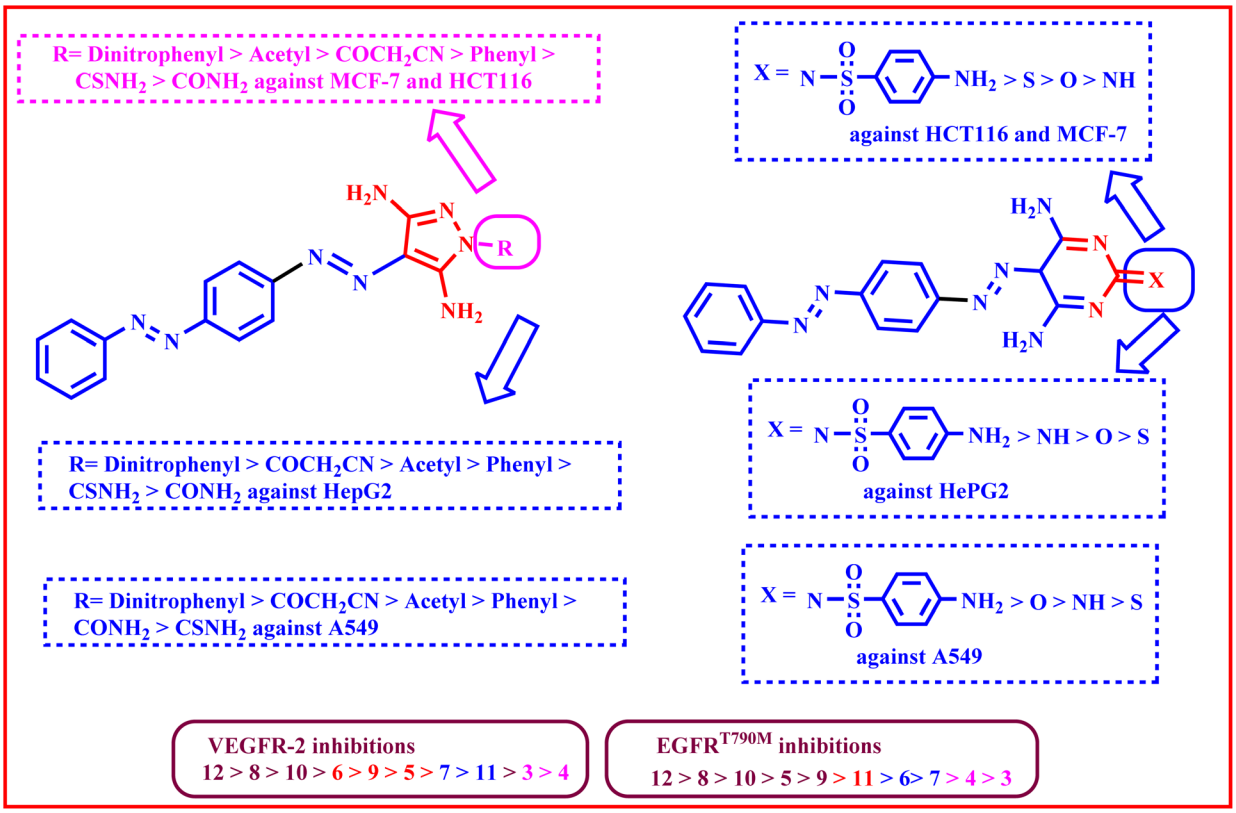

Fig. 13 Schematic presentation for the SAR study.

and 0.40 μM, respectively. Derivative **11** exhibited good inhibition, with IC_{50} = 0.50 μM. Also, structures **6** and **7** gave moderate inhibitions, with IC_{50} = 0.54 and 0.62 μM, respectively. Also, structures **3** and **4** showed lower inhibitions, with IC_{50} = 1.60 and 1.45 μM, respectively.

3.4.4. Structure–activity relationship (SAR). Generally, the pyrimidine derivatives showed higher activities than the pyrazole ones. The elongation of the structure played an important role in their anticancer activity. The obtained structures can be divided into two groups.

The first group of pyrazole derivatives includes compounds **3**, **4**, **5**, **6**, **7** and **8**. In this group, derivative **8**, with the dinitrophenyl moiety, displayed higher cytotoxicity than derivative **6** with the acetyl group, derivative **5** with $COCH_2CN$, derivative **7** with an unsubstituted phenyl group, derivative **3** with $CSNH_2$, and derivative **4** with $CONH_2$ against HCT116 and MCF-7 cells. Conversely, the order of activity against HepG2 cells is **8** > **5** > **6** > **7** > **3** > **4**, while that against A549 cells is **8** > **5** > **6** > **7** > **4** > **3** (Fig. 13).

The second group of pyrimidine derivatives includes compounds **9**, **10**, **11** and **12**. In this group, derivative **12**, with a sulfanilamide moiety, showed higher anticancer activities than pyrimidine-2(5*H*)-thione derivative **10**, pyrimidine-2(5*H*)-one derivative **9** and pyrimidine-2(5*H*)-imine derivative **11** against HCT116 and MCF-7 cells. Conversely, the order of activity is **12** > **11** > **9** > **10** against HepG2 cells, while against A549 cells, the order of activity is **12** > **9** > **11** > **10**.

In addition, pyrimidine derivative **12**, with sulfanilamide, displayed better dual VEGFR-2 and $EGFR^{T790M}$ inhibitions than pyrazole derivative **8** with dinitrophenyl and pyrimidin-2-thione derivative **10**. This could be because the sulfanilamide moiety formed two extra H bonds with Asparagine923 and Leucine840 in the ATP binding domain, while dinitrophenyl formed two extra H bonds with Cysteine919 and Glycine922, but pyrimidin-2-thione derivative **10** formed no extra H bonds.

Derivative **5** exhibited good VEGFR-2 inhibition: **5** > **6** > **9**. Conversely, compounds **7** and **11** displayed moderate inhibitions, while compounds **3** and **4** displayed low inhibitions (Fig. 13).

In the same manner, compounds **5** and **9** displayed very good $EGFR^{T790M}$ inhibitions, while derivative **11** exhibited good inhibition. Conversely, compounds **6** and **7** displayed moderate inhibitions, while derivatives **3** and **4** showed low inhibitions (Fig. 13).

3.5. *In silico* ADMET profile

In silico ADMET predictions were carried out for the most potent compounds **8**, **10** and **12** and correlated to Lipinski's rule of five.[59] Calculations were achieved using the pkCSM descriptor algorithm.[60] For good absorption, our derivatives should adhere to at least three of the following rules: (i) no more than 5H-bond donors, (ii) a log *P* less than 5, (iii) a molecular weight less than 500, and (iv) no more than 10H-bond acceptors. Sorafenib

Table 5 ADMET profiles of the most effective compounds (**8**, **10** and **12**), sorafenib and erlotinib

Parameter	**8**	**10**	**12**	Sorafenib	Erlotinib
Physicochemical properties					
log *P*	5.6839	3.5672	3.6094	5.5497	3.4051
Molecular weight	472.425	350.411	488.537	464.831	393.443
Donors	2	2	3	3	1
Acceptors	12	7	9	4	7
Rotatable bonds	7	4	6	5	10
Absorption					
Human intest. absorption	97.026	89.224	80.283	89.043	94.58
Distribution					
CNS permeability	−2.043	−2.101	−2.379	−2.007	−3.216
BBB permeability	−1.71	−0.835	−1.182	−1.684	−0.745
Metabolism					
CYP2D6 substrate	No	No	No	No	No
CYP3A4 substrate	Yes	Yes	Yes	Yes	Yes
Inhibition of CYP1A2	No	Yes	Yes	Yes	Yes
Inhibition of CYP2C19	Yes	No	Yes	Yes	Yes
Inhibition of CYP2C9	Yes	No	Yes	Yes	Yes
Inhibition of CYP2D6	No	No	Yes	No	No
Inhibition of CYP3A4	Yes	No	No	Yes	Yes
Excretion					
Clearance	−0.536	0.321	−0.658	−0.219	0.702
Toxicity					
Chronic toxic activity (LOAEL)	1.061	0.884	2.172	1.198	1.37
Acute toxic activity (LD_{50})	2.566	2.415	2.687	2.538	2.393
Hepatotoxic effect	Yes	No	Yes	Yes	Yes

violated one rule, and derivative **8** violated two rules, but erlotinib did not violate any rules.

Derivatives **8** and **10** exhibited excellent human intestinal absorption (97.026 and 89.224, respectively), and derivative **12** exhibited very good absorption (80.283), indicating that they can cross numerous biological membranes[61] (Table 5). So through GIT, they might display a meaningfully high bioavailability. Our compounds can reach the CNS (CNS permeability range: −2.043 to −2.379), which may be attributed to their high lipophilicity (log *P* = 3.5672–5.6839).

It is commonly known that sorafenib and erlotinib can hinder drug metabolism through CYP3A4 inhibition, but our derivatives **10** and **12** cannot. The predicted elimination can be correlated with the total clearance, which is important for estimating dosing intervals. Erlotinib presented higher clearance rates than sorafenib and our compounds. Erlotinib needs shorter dosing intervals as it is removed more quickly. In contrast to erlotinib, our compounds indicated broader dosing windows and prolonged half-life, as they have lower clearance rates. Hepatotoxicity was demonstrated by sorafenib, erlotinib and compounds **8** and **12**, while derivative **10** did not exhibit this unwanted hepatotoxic effect. Lastly, the acute toxic doses of erlotinib and sorafenib are similar to those of our compounds. Moreover, the oral chronic toxic doses of compound **12** are higher than those of both erlotinib and sorafenib, while derivatives **8** and **10** exhibited lower doses.

4. Conclusion

Novel pyrazole/pyrimidine derivatives substituted with azobenzenes were synthesized using microwave and traditional methods. Our compounds were assessed for cytotoxicity against HepG2, MCF-7, HCT-116 and A549 cells as dual inhibitors for $EGFR^{T790M}$ and VEGFR-2. A docking study was carried out to show the binding affinities and orientations of our derivatives in the active sites of VEGFR-2 and $EGFR^{T790M}$. The data of the docking study were highly correlated with the biological data, where high binding affinities towards both VEGFR-2 and $EGFR^{T790M}$ receptors were obtained for compounds **12**, **8** and **10**. These compounds exhibited the highest cytotoxicity and VEGFR-2/$EGFR^{T790M}$ inhibition assays. The obtained data concluded that the presence of azobenzene linkers augmented the cytotoxicity of pyrazole and pyrimidine derivatives, which may be attributed to the hydrophobic interactions between this azobenzene scaffold and the hydrophobic pockets in the $EGFR^{T790M}$ and VEGFR-2 receptors. The HCT116 and A549 cell lines were extremely affected by our derivatives. Compound **12** exhibited the highest potency against A549, HepG2, MCF-7, and HCT116 cancer cell lines, with IC_{50} = 5.12, 6.77, 5.85, and 5.25 μM, respectively. It presented higher cytotoxicity than erlotinib (IC_{50} = 5.49, 7.73, 8.20, and 13.91 μM, respectively) and showed lower cytotoxicity than sorafenib (IC_{50} = 4.04, 4.00, 5.58, and 5.05 μM, respectively). Against the HCT116 cell lines,

compounds **5**, **6**, **7**, **8**, **9** and **10**, with IC_{50} = 6.00–8.25 μM, offered very good cytotoxicity. Against the MCF-7 cell lines, derivatives **5**, **6**, **7**, **8**, **9** and **10**, with IC_{50} = 7.15–8.60 μM, offered very good cytotoxicity. With regard to the HepG2 cell lines, derivatives **5**, **6**, **8**, **9** and **11**, with IC_{50} = 7.85–9.75 μM, offered very good cytotoxicity. Against the A549 cell lines, compounds **5**, **6**, **7**, **8**, **9**, **10** and **11**, with IC_{50} = 6.10–8.80 μM, offered very good cytotoxicity. Moreover, the cytotoxicity of the significantly potent derivatives **5**, **6**, **8**, **9**, **10** and **12** against the MCF-10 healthy cell lines was evaluated. The estimated structures indicated low toxicity against MCF-10 cells, with IC_{50} = 50.90–55.50 μM. Compounds **5**, **6**, **8**, **9**, **10** and **12** exhibited 8.09-, 6.53-, 8.92-, 7.30-, 8.10- and 10.57-fold higher toxicity against HCT-116 cells, respectively, than against MCF-10 cells. Equivalently, derivatives **5**, **6**, **8**, **9**, **10** and **12** exhibited 7.28-, 6.44-, 7.48-, 7.17-, 7.16- and 9.49-fold higher toxicity against MCF-7 cells, respectively, than against healthy MCF-10 cells. In addition, derivatives **5**, **6**, **8**, **9**, **10** and **12** exhibited 6.94-, 5.22-, 7.28-, 6.57-, 6.84- and 8.20-fold higher toxicity against HepG2 cells, respectively, than against MCF-10 cells. Also, derivatives **5**, **6**, **8**, **9**, **10** and **12** exhibited 7.64-, 6.74-, 8.77-, 7.22-, 7.58- and 10.84-fold higher toxicity against A549 cells, respectively, than against MCF-10 cells. Furthermore, all compounds were tested for dual $EGFR^{T790M}$ and VEGFR-2 inhibitions. Amongst them, derivatives **12**, **8** and **10** showed very good VEGFR-2 inhibitions, with IC_{50} = 0.90, 0.95 and 1.00 μM, respectively. Similarly, structures **12**, **8**, **10**, **5** and **9** showed strong $EGFR^{T790M}$ inhibitions, with IC_{50} = 0.25, 0.30, 0.33, 0.35 and 0.40 μM, respectively. In addition, *in silico* ADMET predictions were calculated for the highly active derivatives **8**, **10** and **12** and correlated to Lipinski's rule of five, using erlotinib and sorafenib as standard ligands. The results presented our derivatives as promising candidates for advanced manipulations to get more potent anticancer agents with advanced VEGFR-2 and $EGFR^{T790M}$ inhibitions.

5. Experimental

5.1. Chemistry

Microwave technique was carried out using "10 mL" borosilicate glass vials under 2–5 bar pressure at 120 °C in an Anton Paar Monowave 300 for 1–5 min. The spectra of ^{1}H NMR and ^{13}C NMR were recorded on Varian Mercury 300 MHz and 100 MHz-NMR spectrometers, respectively. 2-(4-(Phenyldiazenyl) phenyldiazenyl)-malononitrile (**2**) was obtained through a recognized method.[42–44]

5.1.1. General method for the synthesis of pyrazole derivatives (3–8). A solution of 2-(4-(phenyldiazenyl)phenyldiazenyl) malononitrile **2** (0.01 mol, 2.74 g) in acetone (15 mL) was refluxed for 5–30 h with the appropriate thiosemicarbazide (0.91 g, 0.1 mol), semicarbazide hydrochloride (1.11 g, 0.1 mol), 2-cyanoacetohydrazide (0.99 g, 0.1 mol), acetohydrazide (0.74 g, 0.1 mol), phenyl hydrazine (1.08 mL, 0.1 mol), and/or 2,4-dinitro phenyl hydrazine (1.98 g, 0.1 mol). After cooling, the solid obtained was collected by filtration. The residue was washed with ethanol and recrystallized from the proper solvent to give compounds **3–8**.

*5.1.1.1. 3,5-Diamino-4-(4-(phenyldiazenyl)phenyldiazenyl)-1H-pyrazole-1-carbothioamide (**3**).* Reddish brown crystal; m.p. 268–270 °C; IR (cm^{-1}): 3395, 3304 (NH_2), 1617 (C=N), 1582, 1516 (N=N), 1224 (C=S); ^{1}H-NMR (300 MHz, DMSO-d_6) δ (ppm): 5.86 (s, 2H, NH_2, D_2O exchangeable), 6.28 (s, 2H, NH_2, D_2O exchangeable), 7.031–7.52 (m, 9H, Ar-H), 10.81 (s, 2H, NH_2, D_2O exchangeable); ^{13}C-NMR (300 MHz, DMSO-d_6) δ (ppm): 76.3, 122.2, 122.9, 123.1, 123.2, 124.1, 124.4, 129.1, 129.4, 129.7, 130.0, 132.0, 138.8, 139.0, 147.8 and 182.9; anal. calcd for $C_{16}H_{15}N_9S$ (365) C, 52.60; H, 4.11; N, 34.52; S, 8.77, found: C, 52.49; H, 4.27; N, 34.61; S, 8.63.

*5.1.1.2. 3,5-Diamino-4-(4-(phenyldiazenyl)phenyldiazenyl)-1H-pyrazole-1-carboxamide (**4**).* Brown crystal; m.p. > 300 °C; IR (cm^{-1}): 3402, 3304, 3207 (NH_2), 1686 (C=O), 1606 (C=N), 1511 (N=N); ^{1}H-NMR (300 MHz, DMSO-d_6) δ (ppm): 5.92 (s, 2H, NH_2, D_2O exchangeable), 6.22 (s, 2H, NH_2, D_2O exchangeable), 7.03–7.52 (m, 9H, Ar-H), 8.73 (s, 2H, NH_2, D_2O exchangeable); ^{13}C-NMR (300 MHz, DMSO-d_6) δ (ppm): 71.6, 119.1, 121.2, 121.3, 122.2, 127.0, 129.0, 129.4, 138.4, 138.8, 144.1, 153.1, 153.7, 154.3 and 158.7; anal. calcd for $C_{16}H_{15}N_9O$ (349): C, 55.01; H, 4.30; N, 36.10; found: C, 54.89; H, 4.44; N, 36.17.

*5.1.1.3. 3-(3,5-Diamino-4-(4-(phenyldiazenyl)phenyldiazenyl)-1H-pyrazol-1-yl)-3-oxopropanenitrile (**5**).* Reddish brown crystal; m.p. 254–256 °C; IR (cm^{-1}): 3443 (NH_2), 2194 (CN), 1657 (C=O), 1626 (C=N), 1599, 1559 (N=N); ^{1}H-NMR (300 MHz, DMSO-d_6) δ (ppm): 2.41 (s, 2H, CH_2), 5.86 (s, 2H, NH_2, D_2O exchangeable), 6.30 (s, 2H, NH_2, D_2O exchangeable), 7.03–7.54 (m, 9H, Ar-H); ^{13}C-NMR (300 MHz, DMSO-d_6) δ (ppm): 21.6, 71.4, 119.9, 122.5, 127.8, 128.9, 129.0, 129.2, 129.3, 129.5, 129.8, 130.0, 131.9, 138.4, 138.8, 140.0, 147.7 and 152.8; anal. calcd for $C_{18}H_{15}N_9O$ (373): C, 57.91; H, 4.02; N, 33.78; found: C, 57.98; H, 3.92; N, 33.69.

*5.1.1.4. 1-(3,5-Diamino-4-(4-(phenyldiazenyl)phenyldiazenyl)-1H-pyrazol-1-yl)ethan-1-one (**6**).* Orange crystal; m.p. 232–234 °C; IR (cm^{-1}): 3425 (NH_2), 1650 (C=O), 1563 (C=N and N=N); ^{1}H-NMR (300 MHz, DMSO-d_6) δ (ppm): 2.90 (s, 3H, CH_3), 6.96 (s, 4H, $2NH_2$, D_2O exchangeable), 7.13–7.54 (m, 9H, Ar-H); ^{13}C-NMR (300 MHz, DMSO-d_6) δ (ppm): 21.6, 63.8, 121.2, 122.3, 123.4, 126.0, 128.9, 129.3, 129.8, 129.9, 131.5, 138.8, 147.7, 152.8 and 152.9; anal. calcd for $C_{17}H_{16}N_8O$ (348): C, 58.62; H, 4.60; N, 32.18; found: C, 58.58; H, 4.62; N, 32.23.

*5.1.1.5. 1-Phenyl-4-(4-(phenyldiazenyl)phenyldiazenyl)-1H-pyrazole-3,5-diamine (**7**).* Orange crystal; m.p. > 300 °C; IR (cm^{-1}): 3474, 3395, 3305 (NH_2), 1617 (C=N), 1594, 1516 (N=N); ^{1}H-NMR (300 MHz, DMSO-d_6) δ (ppm): 6.88 (s, 2H, NH_2, D_2O exchangeable), 6.94 (s, 2H, NH_2, D_2O exchangeable), 7.03–7.70 (m, 14H, Ar-H); ^{13}C-NMR (300 MHz, DMSO-d_6) δ (ppm): 63.6, 118.9, 121.2, 121.3, 122.2, 122.6, 123.8, 124.2, 127.9, 129.1, 129.3, 135.9, 138.5, 138.8, 147.0, 147.1, 147.4, 152.7, 153.8 and 153.9; anal. calcd for $C_{21}H_{18}N_8$ (382): C, 65.97; H, 4.71; N, 29.32, found: 66.04; H, 4.65; N, 29.31.

*5.1.1.6. 1-(2,4-Dinitrophenyl)-4-(4-(phenyldiazenyl)phenyldiazenyl)-1H-pyrazole-3,5-diamine (**8**).* Black crystal; m.p. > 300 °C; IR (cm^{-1}): 3423 (NH_2), 1512 (C=N), 1538 (N=N); ^{1}H-NMR (300 MHz, DMSO-d_6) δ (ppm): 7.13–7.85 (m, 12H, Ar-H), 8.04 (s, 2H, NH_2, D_2O exchangeable), 8.06 (s, 2H, NH_2, D_2O

exchangeable); ^{13}C-NMR (300 MHz, DMSO-d_6) δ (ppm): 71.3, 118.4, 119.0, 120.0, 121.3, 122.0, 122.9, 123.1, 123.2, 124.1, 124.4, 129.1, 129.4, 129.7, 130.0, 132.0, 138.8, 139.0, 147.8, 151.0 and 151.6; anal. calcd for $C_{21}H_{16}N_{10}O_4$ (472): C, 53.39; H, 3.39; N, 29.66; found: C, 53.46; H, 3.30; N, 29.71.

5.1.2. General method for synthesis of pyrimidine derivatives (9–12). A solution of 2-((4-(phenyldiazenyl)phenyl)diazenyl)malononitrile **2** (0.01 mol, 2.74 g) in DMF (20 mL) was refluxed in a water bath for 6–12 h with the appropriate urea (0.6 g, 0.1 mol), thiourea (0.76 g, 0.1 mol), guanidine hydrochloride (0.95 g, 0.1 mol), and/or sulfaguanidine (2.14 g, 0.1 mol). After cooling, the mixture was poured into ice water (100 mL); the formed solid was filtered off, washed with water, and recrystallized from the proper solvent to give compounds **9–12**.

*5.1.2.1. 4,6-Diamino-5-(4-(phenyldiazenyl)phenyldiazenyl)pyrimidin-2(5H)-one (**9**).* Black crystal; m.p. 280–282 °C; IR (cm^{-1}): 3369, 3262, 3180 (NH_2), 1643 (C=O), 1619 (C=N), 1531 (N=N); ^{1}H-NMR (300 MHz, DMSO-d_6) δ (ppm): 2.36 (s, 1H, CH–N=N), 5.92 (s, 2H, NH_2, D_2O exchangeable), 6.22 (s, 2H, NH_2, D_2O exchangeable), 7.03–7.52 (m, 9H, Ar-H); ^{13}C-NMR (300 MHz, DMSO-d_6) δ (ppm): 71.9, 114.6, 118.4, 121.3, 127.8, 129.0, 138.4, 144.0, 148.0, 153.1, 153.7, 154.2 and 158.8; anal. calcd for $C_{16}H_{14}N_8O$ (334): C, 57.49; H, 4.19; N, 33.53; found: C, 57.54; H, 4.23; N, 33.47.

*5.1.2.2. 4,6-Diamino-5-(4-(phenyldiazenyl)phenyldiazenyl) pyrimidine-2(5H)-thione (**10**).* Black crystal; m.p. 274–276 °C; IR (cm^{-1}): 3397 (NH_2), 1625, 1617 (C=N), 1555 (N=N), 1266 (C=S); ^{1}H-NMR (300 MHz, DMSO-d_6) δ (ppm): 2.40 (s, 1H, CH–N=N), 5.82 (s, 2H, NH_2, D_2O exchangeable), 6.32 (s, 2H, NH_2, D_2O exchangeable), 6.87–7.54 (m, 9H, Ar-H); ^{13}C-NMR (300 MHz, DMSO-d_6) δ (ppm): 79.2, 121.2, 121.3, 122.2, 127.0, 129.0, 129.4, 138.4, 138.8, 144.1, 147.9, 153.1, 153.7, 154.3 and 178.7; anal. calcd for $C_{16}H_{14}N_8S$ (350): C, 54.86; H, 4.00; N, 32.00; S, 9.14; found: C, 54.79; H, 4.06; N, 31.92; S, 9.23.

*5.1.2.3. 2-Imino-5-(4-(phenyldiazenyl)phenyldiazenyl)-2,5-dihydropyrimidine-4,6-diamine (**11**).* Brown crystal; m.p. 264–266 °C; IR (cm^{-1}): 3461, 3417 (NH_2 and NH), 1512 (C=N), 1538 (N=N); ^{1}H-NMR (300 MHz, DMSO-d_6) δ (ppm): 2.31 (s, 1H, CH–N=N), 6.84 (s, 2H, NH_2, D_2O exchangeable), 6.87 (s, 2H, NH_2, D_2O exchangeable), 7.15–7.99 (m, 9H, Ar-H), 9.14 (s, 1H, NH, D_2O exchangeable); ^{13}C-NMR (300 MHz, DMSO-d_6) δ (ppm): 65.7, 120.5, 121.2, 122.7, 127.0, 128.8, 132.1, 132.2, 135.5, 136.1, 143.2, 144.2, 150.4, 151.3, 155.3, and 156.3; anal. calcd for $C_{16}H_{15}N_9$ (333): C, 57.66; H, 4.50; N, 37.84, found: C, 57.69; H, 4.51; N, 37.80.

*5.1.2.4. 4-Amino-N-(4,6-diamino-5-(4-(phenyldiazenyl)phenyldiazenyl)pyrimidin-2(5H)-ylidene) benzenesulfonamide (**12**).* Reddish brown crystal; m.p. 226–228 °C; IR (cm^{-1}): 3439 (NH_2), 1620 (C=N), 1539 (N=N); ^{1}H-NMR (300 MHz, DMSO-d_6) δ (ppm): 2.41 (s, 1H, CH–N=N), 5.86 (s, 2H, NH_2, D_2O exchangeable), 6.30 (s, 2H, NH_2, D_2O exchangeable), 6.86–7.89 (m, 13H, Ar-H), 7.96 (s, 2H, NH_2, D_2O exchangeable); ^{13}C-NMR (300 MHz, DMSO-d_6) δ (ppm): 66.0, 118.4, 120.1, 120.7, 121.0, 121.3, 122.5, 127.8, 129.0, 129.3, 130.3, 131.5, 138.4, 139.0, 154.0, 162.4, 162.4, 162.8, 166.1 and 166.5; anal. calcd for $C_{22}H_{20}N_{10}SO_2$ (488): C, 54.10; H, 4.10; N, 28.69; S, 6.56, found: C, 54.03; H, 4.14; N, 28.73; S, 6.48.

Conflicts of interest

There is no interest to declare.

Data availability

The data supporting this article are available upon request.

Supplementary information (SI) is available. See DOI: https://doi.org/10.1039/d5ra08997b.

Acknowledgements

This work was funded by the Deanship of Graduate Studies and Scientific Research at Jouf University under grant no. DGSSR-2025-01-01639.

References

1 A. A. Alotaibi, H. H. Asiri, A. F. M. M. Rahman and M. M. Alanazi, Novel pyrrolo[2,3-d]pyrimidine derivatives as multi-kinase inhibitors with VEGFR-2 selectivity, *J. Saudi Chem. Soc.*, 2023, **27**(5), 101712, DOI: 10.1016/j.jscs.2023.101712.

2 I. A. Y. Ghannam, A. M. El Kerdawy, M. M. Mounier, M. T. Abo-elfadl and I. H. Ali, Novel 2-oxo-2-phenylethoxy and benzyloxy diaryl urea hybrids as VEGFR-2 inhibitors: Design, synthesis, and anticancer evaluation, *Arch. Pharm.*, 2023, **356**(2), 2200341, DOI: 10.1002/ardp.202200341.

3 N. S. Aparna, S. S. Aswani, M. S. Mohan, P. T. Boban and S. Kamalamma, Sesamol inhibits LPS induced angiogenesis via downregulating VEGFA/VEGFR2 signalling both in vitro and in vivo, *Pharmacol. Res. Mod. Chin. Med.*, 2023, **9**, 100302, DOI: 10.1016/j.prmcm.2023.100302.

4 U. Acar Çevik, I. Celik, Ş. Görgülü, Z. D. Şahin Inan, H. E. Bostancı, Y. Özkay and Z. A. Kaplacıklı, New benzimidazole-oxadiazole derivatives as potent VEGFR-2 inhibitors: Synthesis, anticancer evaluation, and docking study, *Drug Dev. Res.*, 2024, **85**(4), e22218, DOI: 10.1002/ddr.22218, PMID: 38825827.

5 N. M. Saleh, M. S. A. El-Gaby, K. El-Adl and N. E. A. Abd El-Sattar, Design, green synthesis, molecular docking and anticancer evaluations of diazepam bearing sulfonamide moieties as VEGFR-2 inhibitors, *Bioorg. Chem.*, 2020, **104**, 104350, DOI: 10.1016/j.bioorg.2020.104350.

6 J. Zhu, T. Guo, Z. Wang and Y. Zhao, Triggered azobenzene-based prodrugs and drug delivery systems, *J. Controlled Release*, 2022, **345**, 475–493, DOI: 10.1016/j.jconrel.2022.03.041.

7 K. El-Adl, A.-H. Abdel-Rahman, A. M. Omar, M. Alswah and N. M. Saleh, *Arch. Pharm.*, 2021, e2100237, DOI: 10.1002/ardp.202100237.

8 V. Gandin, A. Ferrarese, M. Dalla Via, C. Marzano, A. Chilin and G. Marzaro, Targeting kinases with anilinopyrimidines: discovery of N-phenyl-N′-[4-(pyrimidin-4-ylamino)phenyl] urea derivatives as selective inhibitors of class III receptor tyrosine kinase subfamily, *Sci. Rep.*, 2015, **5**, 16750.

9 D. M. Wanode and P. B. Khedekar, Synthetic advances and SAR insights of pyrazole-based VEGFR-2 kinase inhibitors, *Med. Drug Discovery*, 2025, **28**, 100227, DOI: 10.1016/j.medidd.2025.100227.

10 H. S. H. Mohamed and S. A. Ahmed, Reviewing of Synthesis and Computational Studies of Pyrazolo Pyrimidine Derivatives, *J. Chem. Rev.*, 2019, **1**(3), 183–232.

11 L. M. Moreno, J. Quiroga, R. Abonia, A. Lauria, A. Martorana, H. Insuasty and B. Insuasty, Synthesis, biological evaluation, and in silico studies of novel chalcone- and pyrazoline-based 1,3,5-triazines as potential anticancer agents, *RSC Adv.*, 2020, **10**, 34114, DOI: 10.1039/D0RA06799G.

12 G. Li, Y. Cheng, C. Han, C. Song, N. Huang and Y. Du, Pyrazole-containing pharmaceuticals: target, pharmacological activity, and their SAR studies, *RSC Med. Chem.*, 2022, **13**(11), 1300–1321, DOI: 10.1039/d2md00206j.

13 N. M. Saleh, M. G. El-Gazzar, H. M. Aly and R. A. Othman, Novel Anticancer Fused Pyrazole Derivatives as EGFR and VEGFR-2 Dual TK Inhibitors, *Front. Chem.*, 2020, **7**, 917, DOI: 10.3389/fchem.2019.00917.

14 S. M. Alhamaky, N. A. Khalil, A. K. A. Bass, N. Osama and M. S. A. Hassan, Design, Synthesis, Docking Studies, and Investigation of Dual EGFR/VEGFR-2 Inhibitory Potentials of New Pyrazole and Pyrazolopyridine Derivatives, *Drug Dev. Res.*, 2025, **86**(1), e70056, DOI: 10.1002/ddr.70056.

15 S. Kumar and B. Narasimhan, Therapeutic potential of heterocyclic pyrimidine scaffolds, *Chem. Cent. J.*, 2018, **12**, 386–398.

16 B. De Filippis, A. Della Valle, A. Ammazzalorso, C. Maccallini, G. Tesse, R. Amoroso, A. Mollica and L. Giampietro, Azobenzene as Multi-Targeted Scaffold in Medicinal Chemistry, *Molecules*, 2024, **29**(24), 5872, DOI: 10.3390/molecules29245872.

17 I. Karakaya, Synthesis and Characterization of Azobenzene Derived from 8-aminoquinoline in Aqueous Media, *J. Turk. Chem. Soc., Sect. A*, 2022, **9**(1), 85–114.

18 L. Giampietro, M. Gallorini, N. Gambacorta, A. Ammazzalorso, B. De Filippis, A. Della Valle, M. Fantacuzzi, C. Maccallini, A. Mollica, A. Cataldi, *et al.*, Synthesis, structure-activity relationships and molecular docking studies of phe-nyldiazenyl sulfonamides as aromatase inhibitors, *Eur. J. Med. Chem.*, 2021, **224**, 113737, DOI: 10.1016/j.ejmech.2021.113737.

19 C. Bustos, L. Alvarez-Thon, E. Molins, I. Moreno-Villoslada, G. Vallejos-Contreras, C. Sánchez, X. Zarate, D. M.-L. Carey and E. Schott, Tuning the molecular/electronic structure of new substituted pyrazoles: Synthesis, biological trials, theoretical approaches and Hammett correlations, *J. Mol. Struct.*, 2018, **1171**, 349–361, DOI: 10.1016/j.molstruc.2018.05.088.

20 S. M. Gomha, A. O. Abdelhamid, N. A. Abdelrehem and S. M. Kandeel, Efficient Synthesis of New Benzofuran-based Thiazoles and Investigation of their Cytotoxic Activity Against Human Breast Carcinoma Cell Lines, *J. Heterocycl. Chem.*, 2018, **55**, 995–1001, DOI: 10.1002/jhet.3131.

21 J. Tang, W. Lu, J. Hu, Y. Jia, X. He, L. Li, S. Yang, Y. Wang and L. Xu, Design, synthesis and biological evaluation of Novel 6-azophenylcoumarin-3-formamido derivatives and a copper(II) complex, *J. Mol. Struct.*, 2024, **1301**, 137448, DOI: 10.1016/j.molstruc.2023.137448.

22 K. Shinzawa, D. Kageta, R. J. Nash, G. W. J. Fleet, T. Imahori and A. Kato, Azobenzene derivatives show anti-cancer activity against pancreatic cancer cells only under nutrient starvation conditions via G0/G1 cell cycle arrest, *Tetrahedron*, 2021, **85**, 132077, DOI: 10.1016/j.tet.2021.132077.

23 A. Sandor, I. Fizesan, I. Ionut, G. Marc, C. Moldovan, I. Oniga, A. Pîrnău, L. Vlase, A. E. Petru, I. Macasoi and O. Oniga, Discovery of A Novel Series of Quinazoline–Thiazole Hybrids as Potential Antiproliferative and Anti-Angiogenic Agents, *Biomolecules*, 2024, **14**(2), 218, DOI: 10.3390/biom14020218.

24 A. M. Srour, N. S. Ahmed, S. S. Abd El-Karim, M. M. Anwar and S. M. El-Hallouty, Design, synthesis, biological evaluation, QSAR analysis and molecular modelling of new thiazol-benzimidazoles as EGFR inhibitors, *Bioorg. Med. Chem.*, 2020, **28**(18), 115657, DOI: 10.1016/j.bmc.2020.115657.

25 N. E. M. Kaufman, S. Dhingra, S. D. Jois and M. D. G. H. Vicente, Molecular Targeting of Epidermal Growth Factor Receptor (EGFR) and Vascular Endothelial Growth Factor Receptor (VEGFR), *Molecules*, 2021, **26**(4), 1076, DOI: 10.3390/molecules26041076.

26 C. Tomuleasa, A. B. Tigu, R. Munteanu, *et al.*, Therapeutic advances of targeting receptor tyrosine kinases in cancer, *Signal Transduction Targeted Ther.*, 2024, **9**, 201, DOI: 10.1038/s41392-024-01899-w.

27 G. M. Nitulescu, G. Stancov, O. C. Seremet, G. Nitulescu, D. P. Mihai, C. G. Duta-Bratu, S. F. Barbuceanu and O. T. Olaru, The Importance of the Pyrazole Scaffold in the Design of Protein Kinases Inhibitors as Targeted Anticancer Therapies, *Molecules*, 2023, **28**(14), 5359, DOI: 10.3390/molecules28145359.

28 R. Dubey, R. Makhija, A. Sharma, A. Sahu and V. Asati, Unveiling the promise of pyrimidine-modified CDK inhibitors in cancer treatment, *Bioorg. Chem.*, 2024, **149**, 107508, DOI: 10.1016/j.bioorg.2024.107508.

29 A. Jug and J. Ilaš, ATP-competitive inhibitors for cancer treatment – kinases and the world beyond, *RSC Med. Chem.*, 2025, **16**(9), 4044–4067, https://api.semanticscholar.org/CorpusID:279604312.

30 A. M. El-Naggar, A. M. A. Hassan, E. B. Elkaeed, M. S. Alesawy and A. Al-Karmalawy, Design, synthesis, and SAR studies of novel 4-methoxyphenyl pyrazole and pyrimidine derivatives as potential dual tyrosine kinase inhibitors targeting both EGFR and VEGFR-2, *Bioorg. Chem.*, 2022, **123**, 105770, DOI: 10.1016/j.bioorg.2022.105770.

31 M. Alsulaimany, A. K. B. Aljohani, N. E. A. Abd El-Sattar, S. A. Almadani, O. M. Alatawi, H. Y. Alharbi, M. S. Aljohani, A. H. Al-Shareef, R. Alghamdi, S. M. Tayeb, D. E. Keshek, K. El-Adl and K. E. Anwer, Dual VEGFR-2 and $EGFR^{T790M}$ inhibitors of phenyldiazenes: anticancer

evaluations, ADMET, docking, design and synthesis, *Future Med. Chem.*, 2025, **17**(3), 287–300, DOI: 10.1080/17568919.2025.2453409.

32 A. M. Sayed, F. A. Taher, M. R. K. Abdel-Samad, M. S. A. El-Gaby, K. El-Adl and N. M. Saleh, Design, synthesis, molecular docking, in silico ADMET profile and anticancer evaluations of sulfonamide endowed with hydrazone-coupled derivatives as VEGFR-2 inhibitors, *Bioorg. Chem.*, 2021, **108**, 104669, DOI: 10.1016/j.bioorg.2021.104669.

33 N. M. Saleh, A. A. Abdel-Rahman, A. M. Omar, M. M. Khalifa and K. El-Adl, Pyridine-derived VEGFR-2 inhibitors: Rational design, synthesis, anticancer evaluations, in silico ADMET profile, and molecular docking, *Arch. Pharm.*, 2021, **354**(8), e2100085, DOI: 10.1002/ardp.202100085.

34 M. Alsulaimany, F. A. Abdulhaleem M., R. Alghamdi, N. E. A. Abd El-Sattar, S. A. Almadani, W. A. Samman, H. Y. Alharbi, M. S. Aljohani, S. M. Tayeb, T. Nasr, K. El-Adl and K. E. Anwer, ADMET, docking, anticancer evaluations, design and synthesis of pyrazolo[1,5-a] pyrimidines substituted with furan and phenyldiazene as dual $EGFR^{T790M}$ and VEGFR-2 inhibitors, *Bioorg. Chem.*, 2025, **163**, 108746, DOI: 10.1016/j.bioorg.2025.108746.

35 M. Alsulaimany, A. K. B. Aljohani, N. E. A. Abd El-Sattar, S. A. Almadani, O. M. Alatawi, H. Y. Alharbi, M. S. Aljohani, A. H. Al-Shareef, R. Alghamdi, S. M. Tayeb, D. E. Keshek, K. El-Adl and K. E. Anwer, Dual VEGFR-2 and $EGFR^{T790M}$ inhibitors of phenyldiazenes: anticancer evaluations, ADMET, docking, design and synthesis, *Future Med. Chem.*, 2025, **17**(3), 287–300, DOI: 10.1080/17568919.2025.2453409, PMID: 39819342, PMCID: PMC11792794.

36 A. K. B. Aljohani, S. S. A. El-Hddad, M. Alsulaimany, N. A. Maghrabi, A. M. Alhammad, M. N. Aloufi, L. F. Alahmadi, T. A. Saeedi, Y. Y. Neyaz, K. E. Anwer, N. E. A. Abd El-Sattar and K. El-Adl, Design, nanogel synthesis, anti-proliferative activity and in silico ADMET profile of pyrazoles and pyrimidines as topo-II inhibitors and DNA intercalators, *RSC Adv.*, 2025, **15**(13), 10037–10048, DOI: 10.1039/d5ra00166h.

37 Q.-Q. Xie, *et al.*, Pharmacophore modeling studies of type I and type II kinase inhibitors of Tie2, *J. Mol. Graphics Modell.*, 2009, **27**(6), 751–758.

38 K. Lee, *et al.*, Pharmacophore modeling and virtual screening studies for new VEGFR-2 kinase inhibitors, *Eur. J. Med. Chem.*, 2010, **45**(11), 5420–5427.

39 V. A. Machado, *et al.*, Synthesis, antiangiogenesis evaluation and molecular docking studies of 1-aryl-3-[(thieno[3,2-b] pyridin-7-ylthio)phenyl]ureas: Discovery of a new substitution pattern for type II VEGFR-2 Tyr kinase inhibitors, *Bioorg. Med. Chem.*, 2015, **23**(19), 6497–6509.

40 F. Sangande, E. Julianti and D. H. Tjahjono, Ligand-Based Pharmacophore Modeling, Molecular Docking, and Molecular Dynamic Studies of Dual Tyrosine Kinase Inhibitor of EGFR and VEGFR2, *Int. J. Mol. Sci.*, 2020, **21**(20), 7779, DOI: 10.3390/ijms21207779.

41 S. A. Elmetwally, K. F. Saied, I. H. Eissa and E. B. Elkaeed, Design, synthesis and anticancer evaluation of thieno[2,3-d]pyrimidine derivatives as dual EGFR/HER2 inhibitors and apoptosis inducers, *Bioorg. Chem.*, 2019, **88**, 102944, DOI: 10.1016/j.bioorg.2019.102944.

42 M. M. Mashaly, A. T. Ramadan, B. A. El-Shetary and A. K. Dawoud, Synthesis and Characterization of New Transition and Actinide Metal Complexes of a Hydrazone Ligand. Mixed-Ligand Complexes, Pyrolysis Products, and Biological Activity, *Synth. React. Inorg. Met.-Org. Chem.*, 2004, **34**(8), 1319–1348.

43 K. E. Anwer, S. S. A. El-Hddad, N. E. A. Abd El-Sattar, A. El-Morsy, F. Khedr, S. Mohamady, D. E. Keshek, S. A. Salama, K. El-Adl and N. S. Hanafy, Five and six membered heterocyclic rings endowed with azobenzene as dual $EGFR^{T790M}$ and VEGFR-2 inhibitors: design, synthesis, in silico ADMET profile, molecular docking, dynamic simulation and anticancer evaluations, *RSC Adv.*, 2023, **13**(50), 35321–35338, DOI: 10.1039/d3ra06614b.

44 M. Alsulaimany, A. K. B. Aljohani, N. E. A. Abd El-Sattar, S. A. Almadani, O. M. Alatawi, H. Y. Alharbi, M. S. Aljohani, A. H. Al-Shareef, R. Alghamdi, S. M. Tayeb, D. E. Keshek, K. El-Adl and K. E. Anwer, Dual VEGFR-2 and $EGFR^{T790M}$ inhibitors of phenyldiazenes: anticancer evaluations, ADMET, docking, design and synthesis, *Future Med. Chem.*, 2025, **17**(3), 287–300, DOI: 10.1080/17568919.2025.2453409.

45 B. M. Essa, A. A. Selim, G. H. Sayed and K. E. Anwer, Conventional and microwave-assisted synthesis, anticancer evaluation, 99mTc-coupling and In-vivo study of some novel pyrazolone derivatives, *Bioorg. Chem.*, 2022, **125**, 105846, DOI: 10.1016/j.bioorg.2022.105846.

46 N. E. A. Abd El-Sattar, E. H. K. Badawy, E. Z. Elrazaz and N. S. M. Ismail, Discovery of pyrano[2,3-d]pyrimidine-2,4-dione derivatives as novel PARP-1 inhibitors: Design, synthesis and antitumor activity, *RSC Adv.*, 2021, **11**(8), 4454–4464, DOI: 10.1039/D0RA10321G.

47 M. K. A. Regal, E. Rafat and N. E. A. Abd El-Sattar, Synthesis, characterization, and dyeing performance of some azo thienopyridine and thienopyrimidine dyes based on wool and nylon, *J. Heterocycl. Chem.*, 2020, **57**(3), 1173–1182, DOI: 10.1002/jhet.3854.

48 K. E. Anwer and G. H. Sayed, Conventional and microwave reactions of 1,3-diaryl-5,4-enaminonitrile-pyrazole derivative with expected antimicrobial and anticancer activities, *J. Heterocycl. Chem.*, 2020, **57**(6), 2339–2353, DOI: 10.1002/jhet.3946.

49 K. E. Anwer, G. H. Sayed and R. M. Ramadan, Synthesis, spectroscopic, DFT calculations, biological activities and molecular docking studies of new isoxazolone, pyrazolone, triazine, triazole and amide derivatives, *J. Mol. Struct.*, 2022, **1256**, 132513, DOI: 10.1016/j.molstruc.2022.132513.

50 F. Khedr, M.-K. Ibrahim, I. H. Eissa, H. S. Abulkhair and K. El-Adl, Phthalazine-based VEGFR-2 inhibitors: Rationale, design, synthesis, in silico, ADMET profile, docking, and anticancer evaluations, *Arch. Pharm.*, 2021, e2100201, DOI: 10.1002/ardp.202100201.

51 M. McTigue, B. W. Murray, J. H. Chen, Y. Deng, J. Solowiej and R. S. Kania, *Proc. Natl. Acad. Sci. U. S. A.*, 2012, **109**, 18281, DOI: 10.1073/pnas.1207759109.

52 S. A. Elmetwally, K. F. Saied, I. H. Eissa and E. B. Elkaeed, Design, synthesis and anticancer evaluation of thieno[2,3-d]pyrimidine derivatives as dual EGFR/HER2 inhibitors and apoptosis inducers, *Bioorg. Chem.*, 2019, **88**, 102944, DOI: 10.1016/j.bioorg.2019.102944.

53 T. Mosmann, Rapid colorimetric assay for cellular growth and survival: application to proliferation and cytotoxicity assays, *J. Immunol. Methods*, 1983, **65**(1–2), 55–63, DOI: 10.1016/0022-1759(83)90303-4.

54 F. M. Freimoser, *et al.*, The MTT [3-(4,5-dimethylthiazol-2-yl)-2,5-diphenyltetrazolium bromide] assay is a fast and reliable method for colorimetric determination of fungal cell densities, *Appl. Environ. Microbiol.*, 1999, **65**(8), 3727–3729.

55 K. El-Adl, *et al.*, Design, synthesis, molecular docking, and anticancer evaluations of 1-benzylquinazoline-2,4(1H,3H)-dione bearing different moieties as VEGFR-2 inhibitors, *Arch. Pharm.*, 2020, e2000068, DOI: 10.1002/ardp.202000068.

56 C. Deng, J. Xiong, X. Gu, X. Chen, S. Wu, Z. Wang, D. Wang, J. Tu and J. Xie, Novel recombinant immunotoxin of EGFR specific nanobody fused with cucurmosin, construction and antitumor efficiency in vitro, *Oncotarget*, 2017, **8**(24), 38568–38580.

57 N. A. A. M. Aziz, R. F. George, K. El-Adl and W. R. Mahmoud, Exploration of thiazolidine-2,4-diones as tyrosine kinase inhibitors: Design, synthesis, ADMET, docking, and antiproliferative evaluations, *Arch. Pharm.*, 2022, e2200465, DOI: 10.1002/ardp.202200465.

58 S. M. Abou-Seri, *et al.*, 1-Piperazinylphthalazines as potential VEGFR-2 inhibitors and anticancer agents: synthesis and in vitro biological evaluation, *Eur. J. Med. Chem.*, 2016, **107**, 165–179.

59 C. A. Lipinski, F. Lombardo, B. W. Dominy and P. J. Feeney, Experimental and computational approaches to estimate solubility and permeability in drug discovery and development settings, *Adv. Drug Delivery Rev.*, 1997, **23**(1–3), 3–25, DOI: 10.1016/S0169-409X(96)00423-1.

60 D. E. V. Pires, T. L. Blundell and D. B. Ascher, pkCSM: Predicting Small-Molecule Pharmacokinetic and Toxicity Properties Using Graph-Based Signatures, *J. Med. Chem.*, 2015, **58**(9), 4066–4072, DOI: 10.1021/acs.jmedchem.5b00104.

61 A. Beig, R. Agbaria and A. Dahan, Oral Delivery of Lipophilic Drugs: The Tradeoff between Solubility Increase and Permeability Decrease When Using Cyclodextrin-Based Formulation, *PLoS One*, 2013, **8**(10), e68237, DOI: 10.1371/journal.pone.0068237.